8. Q-Switching

A mode of laser operation extensively employed for the generation of high pulse power is known as Q-switching. It has been so designated because the optical Q of the resonant cavity is altered when this technique is used [8.1, 2]. As was discussed in Chap. 3, the quality factor Q is defined as the ratio of the energy stored in the cavity to the energy loss per cycle. Consequently, the higher the quality factor, the lower the losses.

In the technique of Q-switching, energy is stored in the amplifying medium by optical pumping, while the cavity Q is lowered to prevent the onset of laser emission. Although the energy stored and the gain in the active medium are high, the cavity losses are also high, lasing action is prohibited, and the population inversion reaches a level far above the threshold for normal lasing action. The time for which the energy may be stored is on the order of τ_f, the lifetime of the upper level of the laser transition. When a high cavity Q is restored, the stored energy is suddenly released in the form of a very short pulse of light. Because of the high gain created by the stored energy in the active material, the excess excitation is discharged in an extremely short time. The peak power of the resulting pulse exceeds that obtainable from an ordinary long pulse by several orders of magnitude.

Figure 8.1 shows a typical time sequence of the generation of a Q-switched pulse. Lasing action is disabled in the cavity by a low Q of the cavity. Toward the end of the flashlamp pulse, when the inversion has reached its peak value, the Q of the resonator is switched to some high value. At this point a photon flux starts to build up in the cavity and a Q-switch pulse is emitted. As illustrated in Fig. 8.1, the emission of the Q-switched laser pulse does not occur until after an appreciable delay, during which time the radiation density builds up exponentially from noise.

8.1 Q-Switch Theory

A number of important features of a Q-switched pulse, such as energy content, peak power, pulse width, rise and fall times, and pulse formation time, can be obtained from the rate equations discussed in Chap. 1. In all cases of interest the Q-switched pulse duration is so short that we can neglect both spontaneous emission and optical pumping in writing the rate equations.

From (1.61, 1.58), it follows that

$$\frac{\partial \phi}{\partial t} = \phi \left(c\sigma n \frac{l}{L} - \frac{\varepsilon}{t_r} \right) \tag{8.1}$$

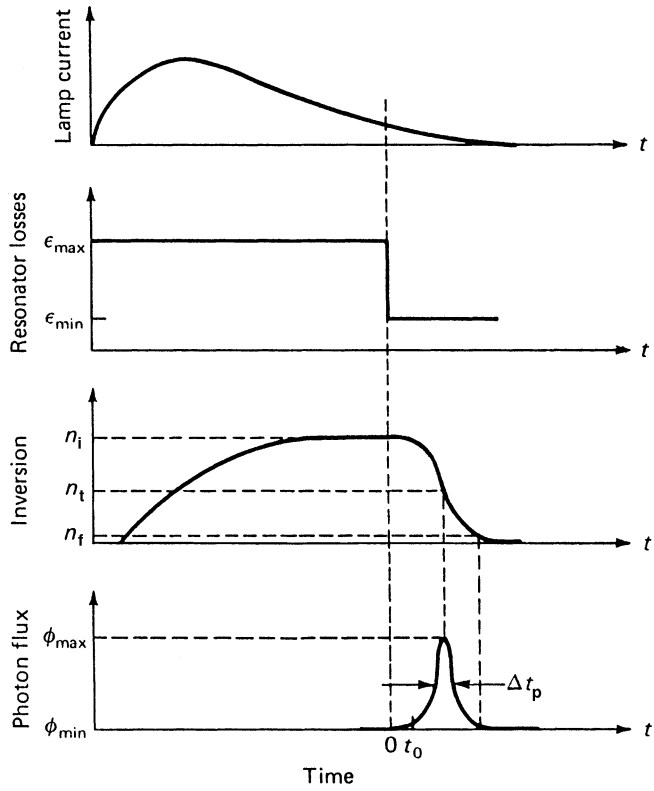

Fig. 8.1. Development of a Q-switched laser pulse. The flashlamp output, resonator loss, population inversion, and photon flux as a function of time are shown.

and

$$\frac{\partial n}{\partial t} = -\gamma n \phi \sigma c. \tag{8.2}$$

In (8.1) we expressed the photon lifetime τ_c by the round-trip time t_r and the fractional loss ε per round trip according to (3.8). Also, a distinction is made between the length of the active material l and the length of the resonator L. Q-switching is accomplished by making ε an explicit function of time (e.g., rotating mirror or Pockels cell Q-switch) or a function of the photon density (e.g., saturable absorber Q-switch). The losses in a cavity can be represented by

$$\varepsilon = -\ln R + \delta + \zeta(t), \tag{8.3}$$

where the first term represents the output coupling losses determined by the mirror reflectivity R, the second term contains all the incidental losses such as scattering, diffraction, and absorption, and $\zeta(t)$ represents the cavity loss introduced by the Q-switch. For a particular explicit form of $\zeta(t, \phi)$, the coupled rate equations can be solved numerically with the boundary condition $\zeta(t < 0) = \zeta_{max}; \zeta(t \geq 0) = 0$. In

many instances Q-switches are so fast that no significant change of population inversion takes place during the switching process; in these cases ζ can be approximated by a step function.

8.1.1 Fast Q-Switch

In the ideal case, where the transition from low Q to high Q is made instantaneously, the solution to the rate equations is particularly simple. In this case we assume that at $t = 0$ the laser has an initial population inversion n_i, and the radiation in the cavity has some small but finite photon density ϕ_i. Initially, the photon density is low while the laser is being pumped and the cavity losses are $\varepsilon_\mathrm{max} = -\ln R + \delta + \zeta_\mathrm{max}$ as illustrated in Fig. 8.1. The losses are suddenly reduced to $\varepsilon_\mathrm{min} = -\ln R + \delta$. The photon density rises from ϕ_i, reaches a peak ϕ_max many orders of magnitude higher than ϕ_i, and then declines to zero. The population inversion is a monotone decreasing function of time starting at the initial inversion n_i and ending at the final inversion n_f. We note that the value for n_f is below the threshold inversion n_t for normal lasing operation. At n_t the photon flux is maximum and the rate of change of the inversion dn/dt is still large and negative, and n falls below the threshold value n_t and finally reaches the value n_f. If n_i is not too far above n_t, that is, the initial gain is close to threshold, then the final inversion n_f is about the same amount below threshold as n_i is above and the output pulse is symmetric. On the other hand, if the active material is pumped considerably above threshold, the gain drops quickly in a few cavity transit times t_r to where it equalizes the losses. After the maximum peak power is reached at n_t, there are enough photons left inside the laser cavity to erase the remaining population excess and drive it quickly to zero. In this case the major portion of the decay proceeds with a characteristic time constant τ_c, which is the cavity time constant.

The equations describing the operation of rapidly Q-switched lasers involve the simultaneous solution of two coupled differential equations for the time rate of change of the internal photon density in the resonator, (8.1), and the population inversion density in the active medium, (8.2). We can express the output energy of the Q-switched laser as follows [8.3]:

$$E_\mathrm{out} = \frac{h\nu A}{2\sigma\gamma} \ln\left(\frac{1}{R}\right) \ln\left(\frac{n_\mathrm{i}}{n_\mathrm{f}}\right), \tag{8.4}$$

where $h\nu$ is the laser photon energy and A is the effective beam cross-sectional area. The initial and final population inversion densities, n_i and n_f, are related by the transcendental equation

$$n_\mathrm{i} - n_\mathrm{f} = n_\mathrm{t} \ln\left(\frac{n_\mathrm{i}}{n_\mathrm{f}}\right), \tag{8.5}$$

where n_t is the population inversion density at threshold, that is,

$$n_\mathrm{t} = \frac{1}{2\sigma l}\left(\ln\frac{1}{R} + \delta\right). \tag{8.6}$$

The pulse width of the Q-switch pulse can also be expressed as a function of the inversion levels, n_i, n_f, n_t,

$$t_p = t_r \frac{n_i - n_f}{n_i - n_t[1 + \ln(n_i/n_t)]}. \tag{8.7}$$

The equations for pulse energy, pulse width, and therefore peak power are expressed in terms of the initial and final population inversion densities, which depend not only on the particular choice of output coupler, but are also related via a transcendental equation.

An analytical solution has been reported in [8.4], which reveals that key parameters such as optimum reflectivity, output energy, extraction efficiency, pulse width, and peak power can all be expressed as a function of a single dimensionless variable

$$z = 2g_0 l/\delta = \ln G_0^2/\delta, \tag{8.8}$$

where $2g_0 l$ is the logarithmic small-signal gain and δ is the round-trip loss.

It is interesting to note that in Chap. 3 we derived expressions for T_{opt}, P_{opt}, and η_E for normal mode operation of the oscillator which were also functions of the parameter z. We will summarize the results of [8.4] because the equations presented in this work are particularly useful to the laser designer. The following expression for the optimum reflectivity was derived

$$R_{opt} = \exp\left[-\delta\left(\frac{z - 1 - \ln z}{\ln z}\right)\right]. \tag{8.9}$$

The energy output for an optimized system is

$$E_{out} = E_{sc}(z - 1 - \ln\ z), \tag{8.10}$$

where E_{sc} is a scale factor with the dimension of energy which contains a number of constants

$$E_{sc} = Ah\nu\delta/2\sigma\gamma,$$

where A is the beam cross section, $h\nu$ is the photon energy, σ is the stimulated emission cross section, δ is the round-trip loss, and γ is one for a four-level laser. The FWHM pulse width versus z is obtained from

$$t_p = \frac{t_r}{\delta}\left(\frac{\ln z}{z[1 - a(1 - \ln a)]}\right), \tag{8.11}$$

where t_r is the cavity round-trip time and $a = (z - 1)/(z\ \ln z)$.

In the limit of large z, the output energy approaches the total useful stored energy in the gain medium

$$E_{st} = \frac{Ah\nu\delta}{2\sigma\gamma} z = \frac{Vh\nu n_i}{\gamma}. \tag{8.12}$$

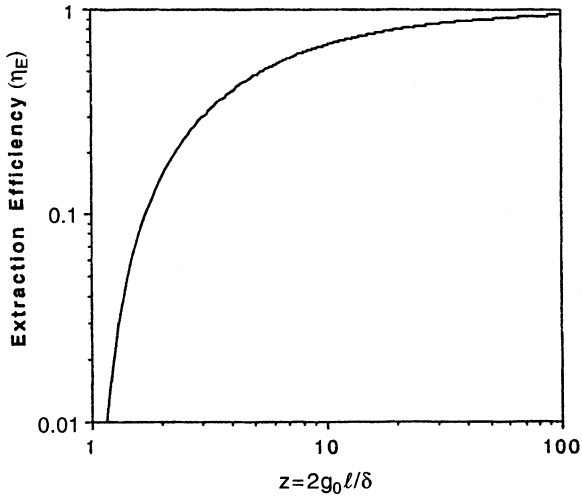

Fig. 8.2. Q-switch extraction efficiency as a function of z.

With (8.10) and (8.12) one can define an energy extraction efficiency

$$\eta_{\mathrm{E}} = 1 - \left(\frac{1+\ln z}{z}\right), \tag{8.13}$$

which is plotted in Fig. 8.2. As one would expect, a high gain-to-loss ratio leads to a high Q-switch extraction efficiency. For a ratio of logarithmic gain to loss of about 10, an extraction efficiency of 70% is achieved. For higher factors of z, the extraction efficiency increases only very slowly.

The reader is reminded that the shape of the curve for η_{E} is similar to the results obtained for the free-running laser discussed in Chap. 3, (see Fig. 3.7), which also depends only on the ratio of $2g_0 l/\delta$. It is also important to remember that besides the Q-switch extraction efficiency expressed by (8.13), the total energy extraction from a Q-switched laser also depends on the fluorescence losses and ASE depopulation losses prior to opening of the Q-switch. The overall efficiency of the Q-switch process has been defined in Sect. 3.4.1 as the product of the Q-switch extraction efficiency, storage efficiency, and depopulation efficiency.

Laser-design trade-offs and performance projections and system optimization can be accomplished quickly with the help of (8.8)–(8.13). For example, we consider the design parameters for a Q-switched Nd:YAG laser with a desired multimode output of 100 mJ. The laser crystal has a diameter of 5 mm and the laser resonator is 30 cm long. Assuming a 5% round-trip cavity loss ($\delta = 0.05$), and with $h\nu = 1.86 \times 10^{-19}$ J and $\sigma = 2.8 \times 10^{-19}$ cm^2, we calculate $E_{\mathrm{sc}} = 3.2 \times 10^{-3}$ J. This requires a ratio of $E_{\mathrm{out}}/E_{\mathrm{sc}} = 30.8$ in order to achieve the desired output energy. From (8.10), one therefore obtains a value $2g_0 l/\delta = 35.4$, or a single-pass power gain of the rod of $G = \exp(g_0 l) = 2.4$. Extraction efficiency follows from (8.13) to be around 87% for $z = 35.4$ and the optimum output coupler has a reflectivity of $R = 0.65$ according to

(8.9). Since the cavity transit round-trip time for the given resonator length is about 2 ns, the expected pulse width from the laser is $t_p = 11$ ns according to (8.11). The peak power of the Q-switch pulse follows from the parameters already calculated and is $P_p = E_{out}/t_p = 9$ MW.

8.1.2 Slow Q-Switching

Instead of a step function, we will now consider the case of a resonator loss that varies in time. A form of Q-switch used in the past is a rotating prism driven by a highspeed motor. A typical spinning rate is 24,000 rpm. At this rate of rotation it takes about 40 ns to sweep over an angle of 0.1 mrad. In this case the cavity loss introduced by Q-switch can be expressed by $\zeta(t) = a \cos \omega t$ in (8.3).

In a slow Q-switch the development of a Q-switch pulse depends on the ratio of pulse build-up time t_D to the switching time. This is illustrated in Fig. 8.3 for three extreme cases. In Fig. 8.3a, the pulse build-up time is longer than the switching time of the Q-switch. The photon flux starts to increase exponentially at $t = 0$, and at the time ϕ_{max} is reached and a pulse is emitted, the Q-switch has already passed the point of ε_{min}. The pulse energy is relatively small because the cavity losses are not at a minimum at the time of maximum photon density. In Fig. 8.3b, Q-switch operation is optimized. The Q-switch is emitted when the cavity losses are minimum, i.e., pulse build-up time and switching times are equal. In Fig. 8.3c, the opening time of the Q-switch is much slower than the pulse build-up time. This leads to the emission of several Q-switched pulses. We note that the first pulse is larger than the second and occurs at a larger value of Δn; the second pulse occurs near the minimum loss level and is much lower in energy. We can explain the occurrence of multiple pulsing as follows: At $t = 0$, the resonator losses are low enough for the photon density to grow exponentially. After 200 ns the photon density has built up to its maximum level and a pulse is emitted. After the pulse is emitted the inversion reaches the

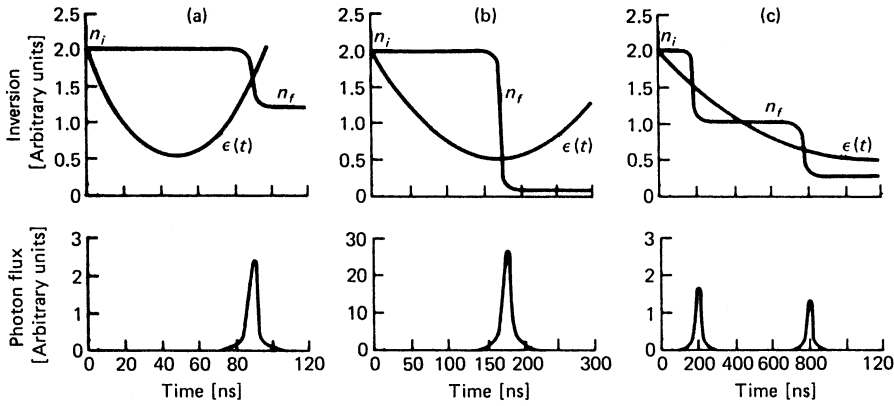

Fig. 8.3. Inversion, cavity losses, and pulse development as a function of time in a slow Q-switched system [8.5]

level n_f. Because n_f is below threshold, the photon density ϕ is very small and a steady state is reached until the slowly changing loss rate term ε decreases enough so that the condition for photon density buildup occurs. The cycle then starts over, but because it now begins with a lower initial value of the inversion a small pulse is produced.

It should be noted that for this multiple pulsing to occur, the first pulse must be emitted at the point of a relatively high loss rate so that another pulse can build up and be emitted when the resonator loss is lower and probably near its minimum.

Multiple pulsing can be avoided either by shortening the switching time of the Q-switch (higher rotational speed) or by increasing the pulse delay time, for example, by increasing the cavity length. From the foregoing consideration it follows that in a laser with fixed pumping level and mirror separation, maximum output is obtained only at one particular speed.

8.1.3 Continuously Pumped, Repetitively Q-Switched Systems

A very important class of laser systems, employed extensively, in micromachining applications, is the cw-pumped, repetitively Q-switched Nd:YAG laser. In these laser systems the population inversion undergoes a cyclic variation, as shown in Fig. 8.4. Between Q-switches the population inversion rises from a value n_f to a value n_i. The buildup of the inversion under the influence of a continuous pumping rate and spontaneous decay is described as a function of time by

$$n(t) = n_\infty - (n_\infty - n_f)\exp\left(-\frac{t}{\tau_f}\right), \tag{8.14}$$

where n_∞ is the asymptotic value of the population inversion, which is approached as t becomes large compared to the spontaneous decay time τ_f. The value n_∞, which depends on the pump input power, is reached only at repetition rates small compared

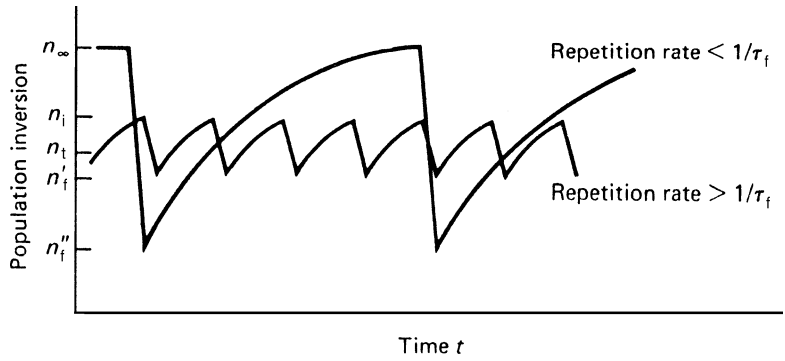

Fig. 8.4. Population inversion versus time in a continuously pumped Q-switched laser; Inversion for two different repetition rates is shown. At repetition rates less than $1/\tau_f$, the inversion approaches the asymptotic value n_∞

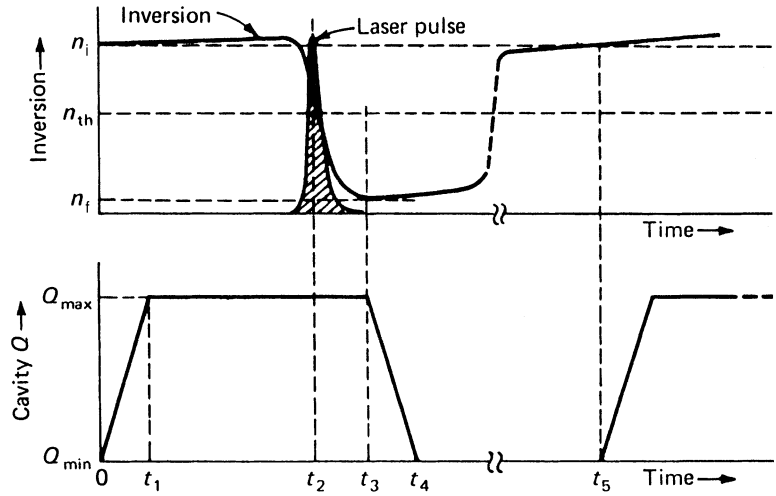

Fig. 8.5. Development of a Q-switched pulse in a cw-pumped system [8.6]

to $1/\tau_f$. For repetition rates larger than $1/\tau_f$, the curves representing the buildup of the population are shorter segments of the same exponential curve followed for the lower repetition rates.

During the emission of a Q-switch pulse, the inversion changes from n_i to n_f. Figure 8.5 shows the development of the Q-switched pulse on an expanded time scale. At $t = 0$, the cavity Q factor starts to increase until it reaches its maximum value Q_{max} at $t = t_1$. Pulse formation ensues until the full pulse output is achieved at $t = t_2$. Stimulated emission ceases at $t = t_3$; at this time continued pumping causes the inversion to start to increase. At the point where the inversion begins to increase, $t = t_3$, the cavity Q begins to decrease, reaching its minimum value at $t = t_4$. During the time period t_3–t_5, the inversion is allowed to build up to its initial value n_i.

The theory of Q-switch operation, summarized at the beginning of this chapter for the case of single Q-switched pulses, can also be applied to the case of repetitive Q-switches, with some modifications that take into account the effects of continuous pumping. Equations (8.1) and (8.2) are applicable; however, we will set $\gamma = 1$ and $n = n_2$ because all repetitively Q-switched lasers of practical use are four-level systems. The inversion levels n_f and n_i are connected by (8.5). During the low-Q portion of the cycle, the inversion n_2 is described by the differential equation

$$\frac{dn_2}{dt} = W_p(n_{tot} - n_2) - \frac{n_2}{\tau_f}. \tag{8.15}$$

With the assumption that $n_2 \ll n_{tot}$ and with

$$n_\infty = W_p \tau_f n_{tot} \tag{8.16}$$

we obtain (8.14) as a solution. For repetitive Q-switching at a repetition rate f, the maximum time available for the inversion to build up between pulses is $1/f$. Therefore,

$$n_{\mathrm{i}} = n_{\infty} - (n_{\infty} - n_{\mathrm{f}}) \exp\left(-\frac{1}{\tau_{\mathrm{f}} f}\right) \tag{8.17}$$

in order for the inversion to return to its original value after each Q-switch cycle.

During each cycle a total energy $(n_{\mathrm{i}} - n_{\mathrm{f}})$ enters the coherent electromagnetic field. Of this a fraction, $T/(T + \delta)$, appears as laser output. Therefore, the Q-switched average power P_{av} at a repetition rate f is given by

$$P_{\mathrm{av}} = \frac{Tf}{T + \delta}(n_{\mathrm{i}} - n_{\mathrm{f}}) h\nu V. \tag{8.18}$$

From the average power and pulse repetition rate follows the energy per pulse, and with the pulse width calculated from (8.7) one obtains the peak power of each pulse. It is convenient to calculate the ratios $P_{\mathrm{p}}/P_{\mathrm{cw}}$ and $P_{\mathrm{av}}/P_{\mathrm{cw}}$, where P_{p} is the Q-switched peak power and P_{cw} is the cw power from the laser at the same pumping level. For cw operation the time derivatives in (8.1) and (8.2) are zero, and we have

$$P_{\mathrm{cw}} = \frac{T}{T + \delta}\left(\frac{n_{\infty} - n_t}{\tau_{\mathrm{f}}}\right) h\nu V. \tag{8.19}$$

Because of the transcendental functions expressed by (8.5), (8.7), and (8.17), the ratios $P_{\mathrm{p}}/P_{\mathrm{cw}}$ and $P_{\mathrm{av}}/P_{\mathrm{cw}}$ cannot be expressed in closed form. The result of numerical calculations is shown in Figs. 8.6 and 8.7.

In Fig. 8.6 the ratio of Q-switched peak power output to the maximum cw output is plotted versus repetition rate for an Nd:YAG laser. For repetition rates below approximately 800 Hz ($\tau_{\mathrm{f}} f \approx 0.20$), the peak power is independent of the repetition rate. At these low repetition rates there is sufficient time between pulses for the inversion to reach the maximum value n_{∞}. In the transition region between 0.8 and 3 kHz, peak power starts to decrease as the repetition rate is increased. Above 3 kHz, the peak power decreases very rapidly for higher repetition rates.

Figure 8.7 shows the ratio of Q-switched average power to cw power as a function of repetition rate. Above a repetition rate of approximately 10 kHz, the Q-switch average power approaches the cw power. At low repetition rates the average power is proportional to the repetition rate. In Fig. 8.8 the experimentally determined peak power, average power pulse width, and pulse buildup time are plotted as a function of repetition rate for an Nd:YAG laser. In accordance with theory, for higher repetition rates the pulse width and the pulse buildup time increase as a result of the reduction of gain.

In the following sections we will describe and compare different Q-switch techniques.

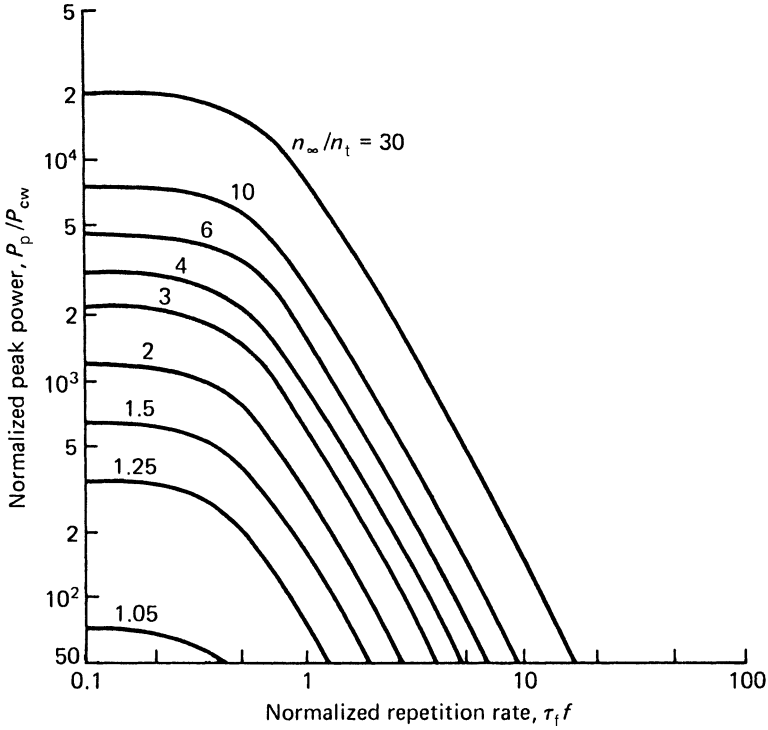

Fig. 8.6. Ratio of peak power to cw power as a function of the repetition rate for a typical cw-pumped Nd:YAG laser. The parameter n_∞/n_t expresses the fractional inversion above threshold [8.7]

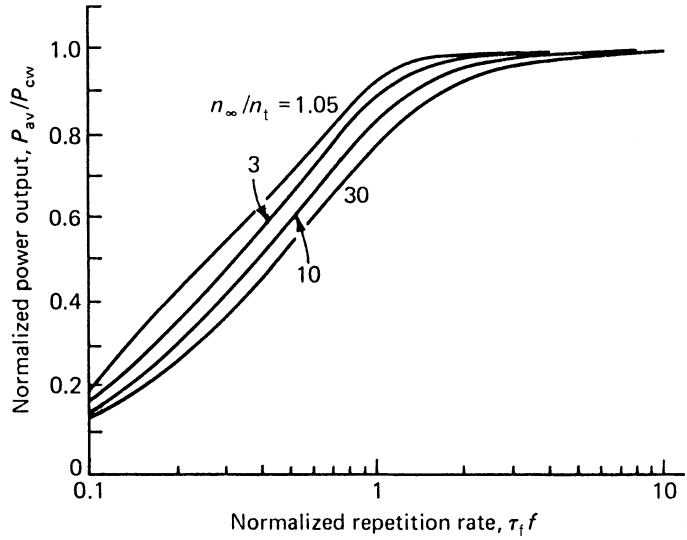

Fig. 8.7. Ratio of Q-switched average power to maximum cw power as a function of normalized repetition rate f [8.7]

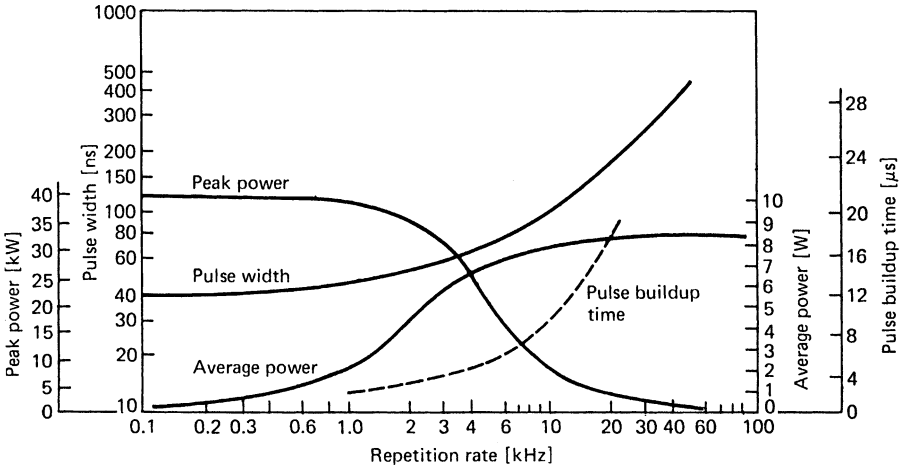

Fig. 8.8. Performance of a cw-pumped Nd:YAG laser system. The peak power, average power, pulse buildup time, and pulse width as a function of repetition rate are plotted

8.2 Mechanical Q-Switches

Q-switches have been designed based upon rotational, oscillatory, or translational motion of optical components. What these techniques have in common is that they inhibit laser action during the pump cycle by either blocking the light path, causing a mirror misalignment, or reducing the reflectivity of one of the resonator mirrors. Near the end of the pump pulse, when maximum energy has been stored in the laser rod, a high Q-condition is established and a Q-switch pulse is emitted from the laser.

The first mechanical Q-switch consisted of nothing more than a rotating disc containing an aperture [8.8]. This method was soon abandoned in favor of rotating mirrors or prisms, which allow much faster switching times [8.9]. In some cases one of the resonator mirrors was attached to one end of a torsional rod driven at its mechanical resonance frequency [8.10]. Minute translations of one mirror have been utilized to change the Q of the cavity. One technique consists of replacing the output mirror of the laser oscillator by a two-plate Fabry–Perot resonator. By modulating the spacing between the two plates, for example, with a piezoelectric transducer, the device can be shifted from a transmission peak to a reflection peak [8.11]. Another technique makes use of frustrated total internal reflection [8.12]. In a FTIR device, a piezoelectric transducer changes the spacing between a roof prism and a second prism. If the two prisms are brought to within a fraction of a wavelength to the surface of the internally reflecting roof prism, the total internal reflection is destroyed. Consequently, the radiation incident on the roof prism is transmitted rather than totally reflected.

The spinning reflector technique for the generation of Q-switched pulses, as shown in Fig. 8.9, involves simply rotating one of the two resonant cavity reflectors so that

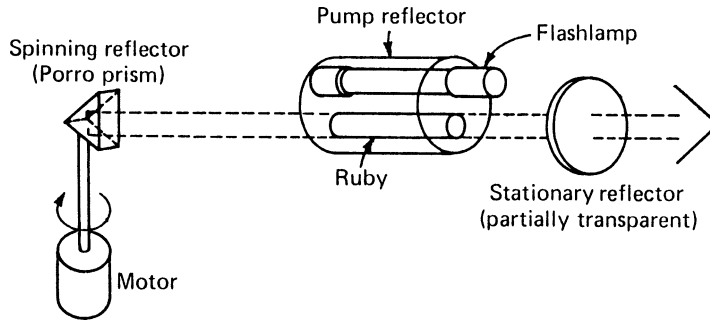

Fig. 8.9. Diagram of a ruby laser employing a spinning prism Q-switch

parallelism of the reflectors occurs for only a brief instant in time. If a plane mirror is employed as the rotating element, the axis of rotation must be aligned to within a fraction of a milliradian parallel to the face of the opposing reflector. This difficulty can be overcome by using a roof prism as the rotating element. If the roof of the prism is perpendicular to the axis of rotation, then the retroreflecting nature of the prism assures alignment in one direction, while the rotation of the prism brings it into alignment in the other direction.

Rotating-mirror devices are simple and inexpensive. They are insensitive to polarization and therefore birefringence effects. Hence, more energy from the laser can be extracted under certain conditions as compared to electro-optic Q-switches. However, the mechanical Q-switches suffer from the tendency to emit multiple pulses. Also, the devices are very noisy and they require frequent maintenance because of the relatively short lifetime of the bearings. Because of these disadvantages the rotating prism Q-switch has been replaced for visible and near infrared lasers by the acousto-optic Q-switch in cw-pumped lasers, and by electro-optic or passive Q-switches in pulsed lasers. However, for Q-switching mid-infrared lasers mechanical devices are still in use. For example 3-μm erbium lasers are frequently Q-switched with rotating prisms [8.13, 14] or with FTIR devices [8.15, 16]. The major disadvantage of Pockels cells is the high switching voltage required at these longer wavelengths.

8.3 Electro-Optical Q-Switches

Very fast electronically controlled optical shutters can be designed by exploiting the electro-optic effect in crystals or liquids. The key element in such a shutter is an electro-optic element that becomes birefringent under the influence of an external field. Birefringence in a medium is characterized by two orthogonal directions called the "fast" and "slow" axes, which have different indices of refraction. An optical beam, initially plane-polarized at 45° to these axes and directed normal to their plane, will split into two orthogonal components, traveling along the same path but at different velocities. Hence, the electro-optic effect causes a phase difference between the two beams. After traversing the medium, the combination of the two components results,

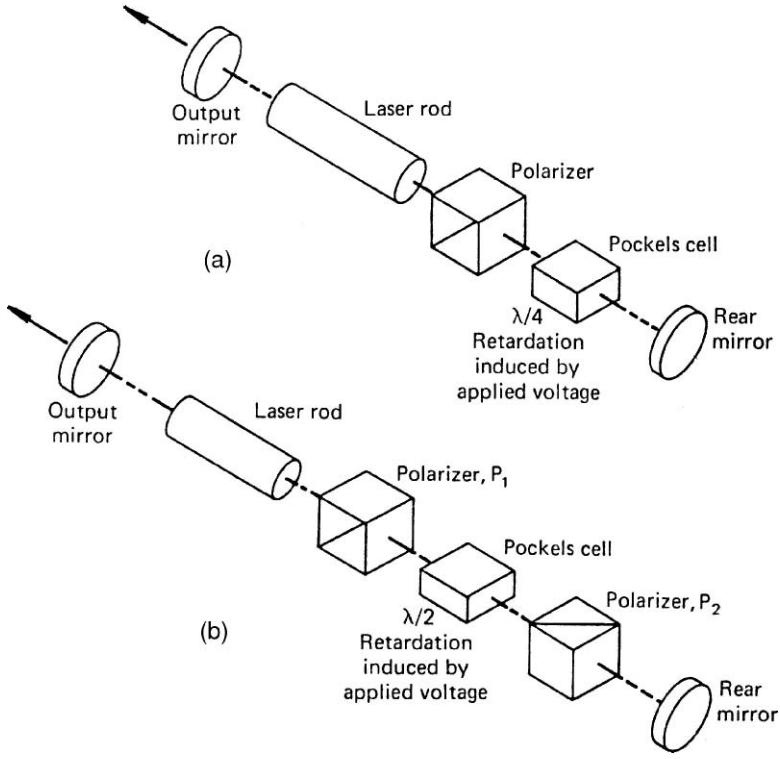

Fig. 8.10. Electro-optic Q-switch operated at (a) quarter-wave and (b) half-wave retardation voltage

depending on the voltage applied, in either an elliptical, circular, or linearly polarized beam. For Q-switch operation only two particular voltages leading to a quarter-wave and half-wave retardation are of interest. In the first case, the incident linearly polarized light is circular polarized after passing the cell, and in the second case the output beam is linearly polarized; however, the plane of polarization has been rotated 90°.

The two most common arrangements for Q-switching are shown in Fig. 8.10. In Fig. 8.10a the electro-optic cell is located between a polarizer and the rear mirror.

The inclusion of the polarizer is not essential if the laser radiation is polarized, for example, in Nd:YLF. The sequence of operation is as follows: During the pump pulse, a voltage $V_{1/4}$ is applied to the electro-optic cell such that the linearly polarized light passed through the polarizer is circularly polarized. After being reflected at the mirror, the radiation again passes through the electro-optic cell and undergoes another $\lambda/4$ retardation, becoming linearly polarized but at 90° to its original direction. This radiation is ejected from the laser cavity by the polarizer, thus preventing optical feedback. Toward the end of the pump pulse the voltage on the cell is switched off, permitting the polarizer–cell combination to pass a linearly polarized beam without loss. Oscillation within the cavity will build up, and after a short delay a Q-switch pulse will be emitted from the cavity.

In the arrangement of Fig. 8.10b an electric voltage must first be applied to the cell to transmit the beam. In this so-called pulse-on Q-switch, the cell is located between two crossed polarizers. As before, polarizer P_1, located between the laser rod and the cell, is not required if the active medium emits a polarized beam. During the pump pulse, with no voltage applied to the cell, the cavity Q is at a minimum due to the crossed polarizers. At the end of the pump pulse, a voltage $V_{1/2}$ is applied to the cell, which causes a 90° rotation of the incoming beam. The light is therefore transmitted by the second polarizer P_2. Upon reflection at the mirror the light passes again through polarizer P_2 and the cell, where it experiences another 90° rotation. Light traveling toward the polarizer P_1 has experienced a 180° rotation and is therefore transmitted through P_1.

There are a number of reasons why it is advantageous to place the Q-switch assembly in front of the rear mirror rather than between the gain medium and the output coupler. First, there is a certain amount of leakage through the Q-switch/polarizer assembly since the extinction ratio is not infinite. A better hold-off of laser radiation, i.e., a lower Q of the resonator, can be achieved if the high reflectivity mirror is blocked by the Q-switch rather than the low reflectivity output coupler. Second, the occurrence of amplified spontaneous emission (ASE) is reduced for the same reason as mentioned above. The feedback loop for potential ASE has a lower reflectivity if the high reflectivity rear mirror is blocked. Third, the peak power in the section between the gain medium and the rear mirror is lower than between the laser crystal and the output coupler, because the circulating power has made only one pass through the gain medium before a fraction is emitted through the output coupler. Since Q-switch assemblies usually have a lower damage threshold than other components, it is advantageous to place these more vulnerable components in the section of the resonator experiencing the lowest peak power.

Two types of electro-optic effects have been used in laser Q-switches: the Pockels effect, which occurs in crystals that lack a center of point symmetry, and the Kerr effect, which occurs in certain liquids. Kerr cells have only been used in the early days of laser technology because they require a voltage that is 5–10 times higher than is required for Pockels cells. The Pockels cell contains an electro-optic crystal in which a refractive index change is produced by an externally applied electric field. Crystals are classified into 32-point groups according to their structure. Only 20-point groups, namely those that lack a center of symmetry, exhibit a nonvanishing electro-optic effect.

The index change produced by an externally applied field is described in each case by a 6×3 matrix of electro-optic coefficients. The number of coefficients is greatly reduced by the structural characteristics of crystals. The most commonly used electro-optic materials have only a few distinct coefficients. The location of a coefficient in the matrix array interrelates the crystal orientation, the applied field direction, and the polarization and direction of the optical beam. The magnitude of each coefficient determines the strength of the electro-optic effect for each geometry.

The basic requirements for a crystal to be useful as an electro-optic Q-switch are a good optical quality combined with a high laser damage threshold and a large electro-optic coefficient for light propagating parallel to the optic axis. The latter requirement

is important because the two-phase-shifted orthogonal components of the beam travel along the same path only if the direction of the light beam is either parallel or normal to the optical axis of the crystal. For other directions the fast and slow axes of the beam include a small angle. Two crystals that meet these criteria and are widely employed in electro-optical Q-switches are potassium dihydrogen phosphate (KDP) and lithium niobate ($LiNbO_3$).

8.3.1 KDP and KD*P Pockels Cells

KDP (KH_2PO_4) and its isomorph KD*P (KD_2PO_4) are grown at room temperature from a water solution that yields large distortion-free single crystals. The attributes of this family of crystals are their high damage threshold and excellent optical quality combined with a large electro-optic coefficient. Crystals with cross sections up to 100 mm have been produced. A disadvantage is the fact that the crystals are fairly soft and hygroscopic and must be protected from the environment by enclosing them in cells that are hermetically sealed or filled with an index-matching fluid. In order to avoid walk-off between the fast and slow beam axes, the electric field has to be applied longitudinally in the same direction as the beam propagation axis and the optical axis of the crystal. The electric field is applied to the crystal by means of a pair of electrodes that contain openings for passage of the laser beam.

Potassium dihydrogen phosphate (KH_2PO_4) or KDP and the deuterated form, which is (KD_2PO_4) or KD*P, are widely used crystals for Pockels cell Q-switches. The latter is usually preferred because of its larger electro-optic coefficient. The dependence of the index of refraction on the electric field can be described in terms of a change in orientation and dimensions of the index ellipsoid. The crystals are uniaxial, that is, in the absence of an electric field the index ellipsoid is an ellipse of revolution about the optic (z) axis. As indicated in Fig. 8.11 the index ellipsoid projects as a circle on a plane perpendicular to the optic axis. The circle indicates that the crystal is not birefringent in the direction of the optic axis. When an electric field is applied parallel to the crystal optic axis, the cross section of the ellipsoid becomes an ellipse with axes x' and y', making a 45° angle with the x and y crystallographic axes. This angle is independent of the magnitude of the electric field. The length of the ellipse axes in the x' and y' directions are proportional to the reciprocals of the indices of refraction in these two directions.

We will now express the phase shift between the orthogonal components corresponding to a wave polarized in the x' and y' directions. Changes of the refractive index Δn are related by the electro-optic tensor r_{ij} of rank 3 to the applied field

$$\Delta\left(\frac{1}{n_i^2}\right) = \sum_{j=1}^{3} r_{ij} E_j, \tag{8.20}$$

where $i = 1, \ldots, 6$ and $j = 1, \ldots, 3$.

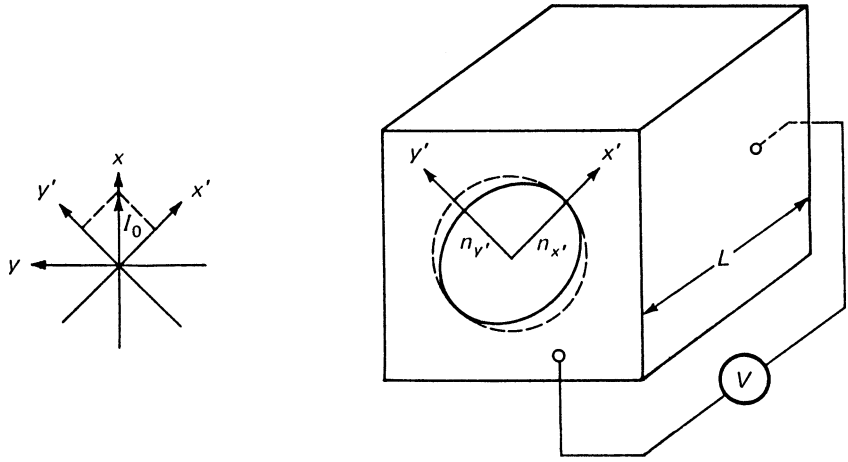

Fig. 8.11. Change of the index ellipsoid in a KDP crystal when an electric field is applied parallel to the z-axis, I_0 is an incident wave polarized in the x direction, x and y are the crystallographic axes, and x' and y' are the electrically induced axes

Generally there exist 18 linear electro-optic coefficients r_{ij}. However, in crystals of high symmetry, many of these vanish. For phosphates of the KDP family, r_{63} is the only independent electro-optic coefficient that describes the changes in the ellipsoid when a longitudinal field is applied to the crystal. The change of refractive index in the x' and y' (directions is [8.17]

$$n_{x'} = n_0 + \frac{1}{2} n_0^3 r_{63} E_z, \qquad n_{y'} = n_0 - \frac{1}{2} n_0^3 r_{63} E_z, \tag{8.21}$$

where n_0 is the ordinary index of refraction and E_z is the electric field in the z direction. The difference in the index of refraction for the two orthogonal components is then

$$\Delta n_0 = n_0^3 r_{63} E_z. \tag{8.22}$$

For a crystal of length l, this leads to a path-length difference $\Delta n_0 l$ and a phase difference of $\Delta\varphi = (2\pi/\lambda)\Delta n_0 l$.

The phase difference $\Delta\varphi$ in a crystal of length l is related to the voltage $V_z = E_z l$ applied across the faces by

$$\Delta\varphi = \frac{2\pi}{\lambda} n_0^3 r_{63} V_z. \tag{8.23}$$

It should be noted that $\Delta\varphi$ is a linear function of voltage and is independent of the crystal dimensions. If linearly polarized light is propagated through the crystal with the direction of polarization parallel to the x- or y-axis, as shown in Fig. 8.11, the components of this vector parallel to the electrically induced axes x' and y' will suffer a relative phase shift $\Delta\varphi$. In general, orthogonal components undergoing a relative phase shift produce elliptically polarized waves. Thus, the application of a voltage in

this configuration changes linearly polarized light to elliptically polarized light. If the light then passes through a polarizer, the resulting light intensity will be a function of the ellipticity and therefore the voltage applied to the crystal. A simple derivation shows that, with the analyzer axis oriented at right angles to the input polarization direction, the voltage and the transmitted light intensity I are related by [8.18].

$$I = I_0 \sin^2 \frac{\Delta\varphi}{2}, \tag{8.24}$$

where I_0 is the input light intensity.

For Q-switch operation, two particular values of phase shift are of interest: these are the $\lambda/4$ and $\lambda/2$ wave retardations that correspond to a phase shift of $\pi/2$ and π. With linearly polarized light being applied, for example, in the x direction, as shown in Fig. 8.11, the output from the crystal is circularly polarized if $\Delta\varphi = \pi/2$. For $\Delta\varphi = \pi$, the output beam is linearly polarized, but the plane of polarization has been rotated 90°.

From (8.23) it follows that the voltage required to produce a retardation of π is

$$V_{\lambda/2} = \frac{\lambda}{2n_0^3 r_{63}}. \tag{8.25}$$

KD*P has an index of refraction of $n_0 = 1.51$ and an electro-optic constant $r_{63} = 26.4 \times 10^{-6}\,\mu\text{m/V}$. With these values we calculate a voltage of $V_{\lambda/2} = 5.8$ kV at 1.06 μm in order to produce a half-wave retardation. Deviations from this voltage will change the transmission $T = I/I_0$ of the Pockels cell according to

$$T = \sin^2\left(\frac{\pi}{2}\frac{V}{V_{\lambda/2}}\right). \tag{8.26}$$

This equation is obtained by combining (8.23–25).

A number of crystals which have been used in Q-switches and electro-optic modulators are listed in Table 8.1. The most widely used crystal is the deuterated form of KH_2PO_4 (KDP), which is KD_2PO_4(KD*P) because it possesses a low half-wave voltage. The crystal CD*A has actually a lower value, but this advantage is offset by a high loss tangent. KD*P and its isomorphs have been characterized in great detail; their properties are reviewed in [8.19–22].

Although the crystals are water-soluble and fragile, they can be handled, cut, and polished without difficulty. The crystals have a high optical transmission in the range of 0.22–1.6 μm, and they possess relatively large electro-optic coefficients.

All crystals listed in Table 8.1 are hygroscopic and must be protected from atmospheric water. This protection is typically provided by enclosing the crystal in a cell which is hermetically sealed or filled with index-matching fluid. As a result, six surfaces are encountered by a laser beam on a single transit through the cell. Transmission losses can be reduced by the use of antireflection coatings on the cell windows. While hard, damage-resistant AR coatings cannot be applied to KDP and its isomorphs, losses at the crystal itself can be very much reduced by the use of an index-matching liquid.

Transmission of typical electro-optic shutters with liquid-immersed crystals and AR-coated windows is about 90%. The electric field is usually applied to the crystal

Table 8.1. Electro-optic parameters of 42 m-type crystals

Material	Index of refraction at 0.55 μm	Electro-optic constant, τ_{63} (μm/V $\times 10^{-6}$)	Typical half-wave voltage (kV) at 0.55 μm
Ammonium dihydrogen phosphate (ADP)	1.53	8.5	9.2
Potassium dihydrogen phosphate (KDP)	1.51	10.5	7.5
Deuterated KDP	1.51	26.4	3.0
Rubidium dihydrogen phosphate (RDP)	1.51	15.5	5.1
Ammonium dihydrogen arsenate (ADA)	1.58	9.2	7.2
Potassium dihydrogen arsenate (KDA)	1.57	10.9	6.5
Rubidium dihydrogen arsenate (RDA)	1.56	14.8	4.9
Cesium dihydrogen arsenate (CDA)	1.57	18.6	3.8
Deuterated CDA	1.57	36.6	2.0

by means of a pair of metal electrodes containing apertures which are either bonded or evaporated onto the square ends of the crystal or simply held in place by compression. The main drawback of end-plate electrodes is their geometry, which gives rise to a nonuniform electric field across the clear aperture. The field strength across the aperture varies from a maximum around the inner edge of the rings to a minimum at the geometric center. Fringing necessitates operation at considerably higher voltages than if the field were uniformly applied. Partial compensation is attained by making the crystal dimension roughly 30% greater than the clear aperture diameter.

A considerable improvement in fringe uniformity can be achieved by using cylindrical band electrodes applied to the end of the barrel of cylindrical-shaped crystals. Band electrodes allow an optical transmission uniformity to within a few percent across the clear aperture. This represents a substantial improvement compared to standard cells containing rectangular crystals and end-plate electrodes.

The electro-optic coefficient of KDP is strongly temperature-dependent. As a consequence, the quarter wave voltage at 1.06 μm increases by approximately 80 V/°C with temperature [8.23]. If large temperature excursions are expected, the voltage of the Pockels cell needs to be adjusted by a feedback loop to provide a stable output energy. Temperature changes of the crystal may be the result of ambient temperatures variations, or they may be caused by absorption losses in the crystal.

The thermally induced nonuniformity of the refractive index caused by the absorption of laser radiation produces birefringence, which can degrade the performance of the Q-switch. The result is a decrease of the transmission of the electro-optic Q-switch when the Q-switch is open. The depolarized component of the intracavity radiation is ejected from the resonator by the polarizer. Also a deviation from the exact quarter wave voltage has the same effect.

In high-average-power Q-switched Nd:YAG lasers, thermally induced birefringence in the Q-switch crystal can be a problem. Similar to the cancellation of thermally induced depolarization in a laser rod, the problem can be solved with two Pockels cells and a polarization rotator inserted between the two electro-optic crystals [8.24].

KDP Pockels cells can also be designed with the electric field perpendicular to the direction of the beam. For this geometry, the half-wave voltage depends on the ratio of thickness to length of the crystal, which has the advantage that by proper choice of the crystal geometry a considerably lower voltage is required as compared to longitudinally applied fields. However in KDP crystals with a transverse field, the propagation direction is at an angle other than normal or parallel to the optic axis. Therefore the extraordinary and ordinary ray propagate in different directions through the crystal. To compensate for this walk-off as well as for temperature effects, two crystals of suitable orientation are usually employed. Because of the need to compensate for the angular and temperature dependence of birefringence in KDP-type crystals, transverse field devices have not become popular as Q-switches in this class of materials.

8.3.2 $LiNbO_3$ Pockels Cells

Lithium niobate is grown from the melt; it is hard and nonhygroscopic. The crystals can be antireflection-coated and do not need a special protection from the environment. Also, the quarter and half-wave voltages are about a factor of 2 lower compared to KD*P. In $LiNbO_3$, the electric field is applied perpendicularly to the beam propagation and optical axis of the crystal. As we will see, this has the advantage of reducing the required voltage by the width to length ratio of the crystal. A drawback of $LiNbO_3$ is that the crystal is available only in relatively small sizes, with cross sections of about 10 mm, and the laser damage threshold is considerably below that of KD*P.

In an arrangement as shown in Fig. 8.12 light propagates along the c-axis of the crystal. If the light is polarized parallel to the a-axis and an electric field is applied parallel to the a axis, the half-wave retardation is [8.25]

$$V_{\lambda/2} = \frac{\lambda d}{2 r_{22} n_0^3 l}, \tag{8.27}$$

where l is the length of the crystal in the c direction, d is the distance between the electrodes along the a-axis, and r_{22} is the electro-optic coefficient.

The half-wave voltage is directly proportional to the distance between the electrodes and inversely proportional to the path length. At a wavelength of $\lambda = 1.064\ \mu m$, the linear electro-optic coefficient is $r_{22} = 5.61 \times 10^{-6}\ \mu m/V$ and the refractive index of the ordinary ray is $n_0 = 2.237$ in $LiNbO_3$. The theoretical half-wave voltage obtained from (8.27) for a typical crystal size of 9 mm × 9 mm × 25 mm is 3.0 kV. The high refractive index of $LiNbO_3$ and the geometrical factor d/l are responsible for the lower voltage requirements of $LiNbO_3$ as compared to KD*P.

The above mentioned half-wave voltage is the value for a dc bias voltage; for pulsed Q-switch operation a slightly higher voltage is usually required. In pulsed

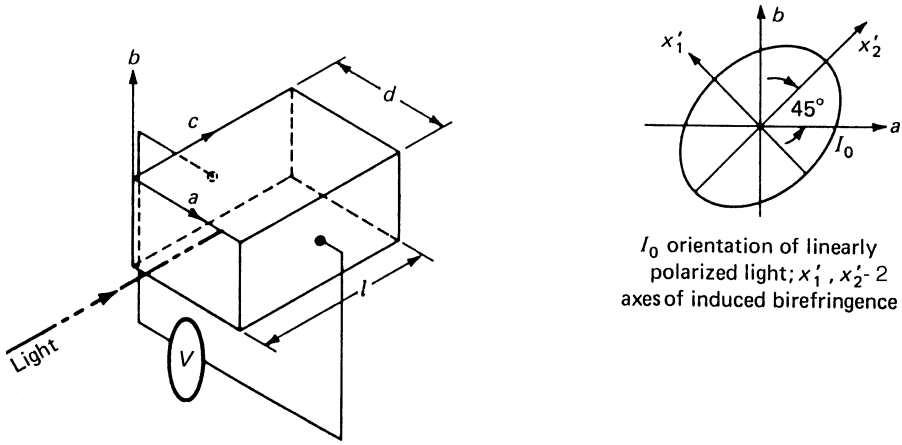

Fig. 8.12. Electro-optic Q-switch employing an $LiNbO_3$ crystal

operations, the value of r_{22} is smaller than for dc operation, which is explained by the fact that for static fields the electro-optic effect is equal to the sum of the intrinsic electro-optic effect and that induced by the piezo-optic effect [8.26]. $r_{22} = r'_{22} + p_{2k}d_{2k}$, where p_{2k} and d_{2k} are the elasto-optic and piezoelectric constants of the crystal. When the bias voltage is turned on or off rapidly, the piezo-optic effect is absent, since deformation of the crystal cannot occur during the fast switching times typical for Q-switch operation.

Output energies of up to 250 mJ are typically obtained from Nd:YAG oscillators containing $LiNbO_3$ Q-switches. The energy extraction is limited by the high gain of this material, which leads to prelasing and subsequently to a depopulation of the inversion. The width of the Q-switched pulses is usually between 10 and 25 ns, and the pulse buildup time is between 50 and 100 ns in typical systems. Generally speaking, the build-up time of the Q-switched pulse is about an order of magnitude larger than the pulse duration, and the Q-switch opening time is shorter than the pulse build-up time.

According to (8.7) the pulse width of a Q-switched laser is a function of the resonator length (t_r) and the gain in the material (n_i). The shortest Q-switch pulses are obtained in very short resonators with the gain medium pumped far above threshold. Small end-pumped Q-switched lasers have generated pulses on the order of a few nanoseconds or less.

For some applications it is desirable to generate relatively long Q-switch pulses. By combining a long resonator with operation close to threshold, pulses as long as 150 ns have been generated. Employing a feedback loop to control the switching of a Pockels cell, pulse durations of up to 1.4 μs have been obtained from Q-switched Nd:YAG lasers [8.27, 28]. The principle of electro-optical feedback control is depicted in Fig. 8.13. The resonator incorporates a Pockels cell as a Q-switching element. Negative feedback to the circulating power is applied by means of the photo-detector-derived voltage on the Pockels cell. In this way the stored energy in the laser rod is released at a controlled rate.

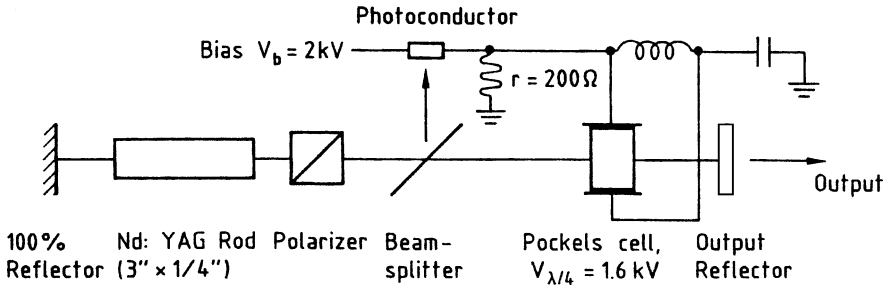

Fig. 8.13. Electro-optic feedback control for stretching of Q-switched pulses [8.27]

In diode-pumped solid-state lasers a fairly rectangular pump pulse is usually generated and the optimum time for Q-switching occurs right at the end of the pump pulse. In flashlamp-pumped systems, the pump pulse can have a relatively long decay time. In this case the maximum extraction energy is obtained if the Q-switch is opened prior to the end of the pump pulse. At the tail end of a slowly decreasing pump pulse, population inversion decreases because the diminishing pump power cannot keep up with the increase of spontaneous emission losses.

The electro-optic coefficients of $LiNbO_3$ are less sensitive to temperature changes as compared to KDP. This is particularly important because $LiNbO_3$ is used in most military rangefinders and target designators which involves operation over a large temperature range. These systems generate between 100 and 250 mJ of output energy and the power density at the Q-switch is on the order of 50 MW/cm^2. Pulse width is 10–20 ns. In these applications crystal temperature may reach 70°C.

The quarter-wave voltage of $LiNbO_3$ is proportional to the laser wavelength according to (8.27). Therefore, very high voltages are required to Q-switch erbium lasers which emit radiation at around 3 μm. $LiNbO_3$ Pockels cells have been successfully used for Q-switching Er:YAG [8.29] and Er:Cr:YSGG [8.15]. However, rapidly switching high voltages produced substantial electromagnetic interference in these lasers.

8.3.3 Prelasing and Postlasing

Theoretically, an infinite loss is introduced into the cavity by a Pockels cell operated at a proper $\lambda/4$ or $\lambda/2$ voltage. In practice, field strength nonuniformities, inhomogeneities in the crystal, birefringence introduced by mechanically clamping the crystal, and nonperfect polarizers limit the extinction ratio of an electro-optic Q-switch to about a hundred. The extinction ratio is defined as the ratio of the maximum to the minimum transmitted intensity obtained between crossed polarizers as the applied voltage is varied through a half-wave voltage.

If the gain of the laser exceeds the loss produced by the Q-switch, normal lasing will occur before the instant of Q-switching. This phenomenon, which is termed "prelasing," is due to the Pockels cell and polarizer combination not acting as a perfect shutter, so that there is still some feedback from the resonator mirror. Prelasing is most

likely to occur just prior to the time of Q-switching since the population inversion, the stored energy, and the gain are largest at that time.

Because of the high gain of Nd:YAG, depopulation of the stored energy by prelasing is a particular problem with this material. Tests have also shown that prelasing may be a major cause of damage to the Pockels cell crystal or polarizers. Prelasing, if it occurs, allows a pulse buildup from a "seed" pulse in a small region of the laser rod. In the area of the laser rod where prelasing occurs, the Q-switched pulse develops more rapidly compared to the rest of the pulse, which must develop from spontaneous emission. As a result, a very high peak power density will occur in this small part of the rod.

Appropriate design precautions must be undertaken to ensure that prelasing does not occur. The first major requirement is to operate the Q-switch at its optimum extinction ratio. This requires that the correct dc bias voltage is applied and that the Pockels cell crystal and polarizers are aligned properly. Typically the optic *c*-axis of the Pockels cell crystal must be parallel to the laser beam direction to within 10 arc min or less. Alignment of the *c*-axis is best performed by centering the optic-axis figure (the Maltese cross pattern) on the resonator optical axis. This is done by illuminating the crystal with a diffuse light source and observing the crystal between crossed polarizers. A pattern of a cross surrounded by a series of circles appears. The line connecting the center of the cross to the point at which the observation is made is exactly parallel to the *c*-axis. Furthermore, to establish the proper condition for Q-switching, the crystal must be aligned so that either the *a*- or *b*-axis is parallel to the polarization direction of the laser ($LiNbO_3$ crystals and longitudinal field KD*P). Figure 8.14 shows the extinction ratio versus bias voltage for a 9 mm $\times$ 9 mm $\times$ 25 mm $LiNbO_3$ crystal.

The main Q-switched pulse may be followed by one or more pulses of lower amplitude (postlasing). The second pulse may occur from several hundred nanoseconds to several tens of microseconds after the main pulse. Postlasing results from piezo-optic effects in the electro-optic crystal. The piezoelectric action of the applied voltage compresses the crystal, and when that voltage is removed the crystal remains compressed for some time. This compression generates a retardation of the optical wave by means of a strain-birefringence effect, thus creating a loss in the cavity which becomes smaller with time as the compression relaxes. Figure 8.15a shows a waveform picture of the voltage conventionally applied to a Pockels cell, and Fig. 8.15b shows the loss versus time for an actual Pockels cell switch. It was found [8.31] that the loss drops to about 25% and then decays to zero in approximately 400 ns. If the resulting decay time of the loss is longer than the output pulse buildup time, the main laser pulse will be emitted before the loss reaches its minimum. Thus some energy will remain in the rod after the first output pulse. This residual energy may produce a second pulse when the cavity loss reaches its minimum. By creating this time-dependent loss, the elasto-optic effect seriously affects the efficiency of a Q-switched laser.

At low input energy levels there is a long time delay between the switching time and the time the output pulse actually appears, as shown in Fig. 8.15c and thus there is negligible loss in efficiency. However, at higher input energy levels the time

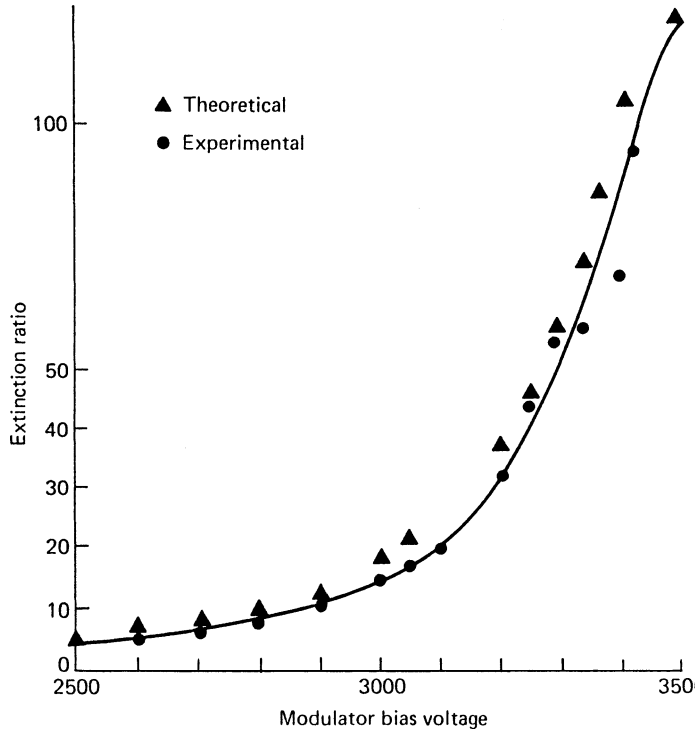

Fig. 8.14. Extinction ratio versus applied voltage of a $LiNbO_3$ Pockels cell-calcite prism assembly [8.30]

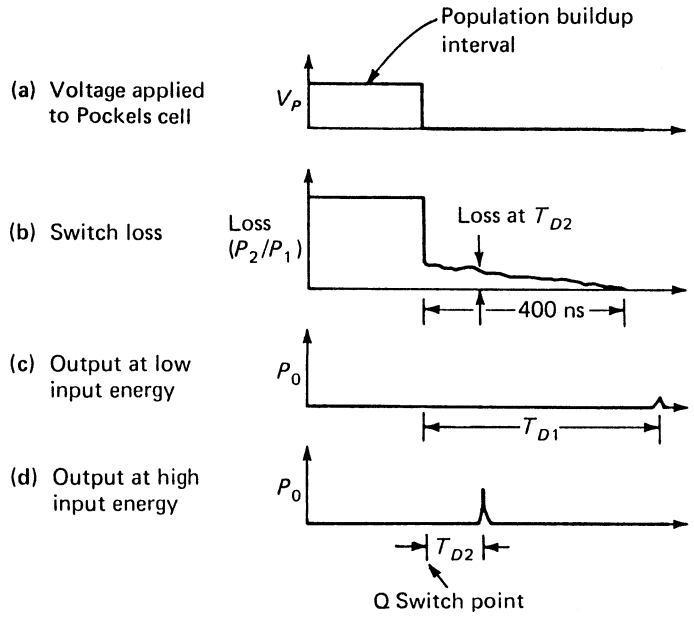

Fig. 8.15. Piezo-optic effect in $LiNbO_3$ [8.31]

delay T_D becomes shorter and thus the laser suffers a considerable output loss due to the switch loss, as shown in Fig. 8.15d. This, besides prelasing, accounts for the roll-off in output efficiency in the Q-switched laser at higher input energy levels.

The elasto-optic effect, which is quite pronounced in $LiNbO_3$ but is also observed in KD*P, can be minimized by switching the bias voltage to a negative value rather than to zero.

KTP, a crystal which is used extensively as an efficient nonlinear-optical crystal, has also been explored as a Q-switch because piezoelectric effects have not been observed in this material [8.32].

8.3.4 Depolarization Losses

In low-repetition-rate systems, or at low input powers, depolarization losses can be ignored, but in higher-average-power systems depolarization losses become significant.

The polarizer, required for Q-switch operation employing a Pockels cell, rejects any radiation not polarized in the proper plane of polarization. This can lead to large depolarization losses in the presence of thermally-induced birefringence, as may occur in high-repetition-rate systems.

Basically the same techniques as dicussed in Sect. 7.1.6 can be employed in order to reduce depolarization losses in electro-optic Q-switched resonators. In large Q-switched oscillators, two laser heads with a 90° phase rotator inserted between the laser rods are sometimes used. In an oscillator containing a single laser head, a Faraday rotator inserted between the laser rod and rear mirror can be employed. Smaller Q-switched oscillators, in particular military lasers, employ mostly a waveplate-Porro prism combination for birefringence compensation. This approach will be discussed in more detail at the end of this section.

Also several techniques have been developed in conjunction with Pockels cell Q-switches which act on both polarizations. In general, the techniques are based on the use of a calcite polarizer in the resonator which separates the two orthogonally polarized beams.

Figure 8.16 shows a calcite polarizer which separates the two orthogonal polarization components into two parallel beams. A quarter-wave plate is inserted into one of the beams, before both beams are passed through a large aperture Pockels cell. A roof prism returns the beams back to the Pockels cell/polarizer assembly [8.33].

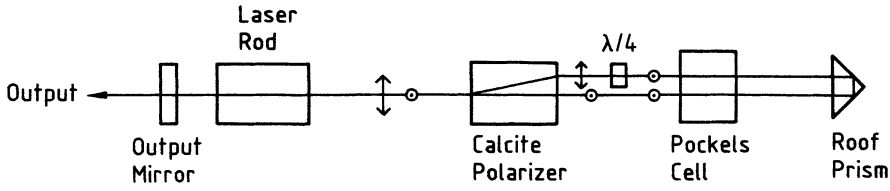

Fig. 8.16. Polarization insensitive Q-switch based on spatial separation of orthogonally polarized beams [8.33]

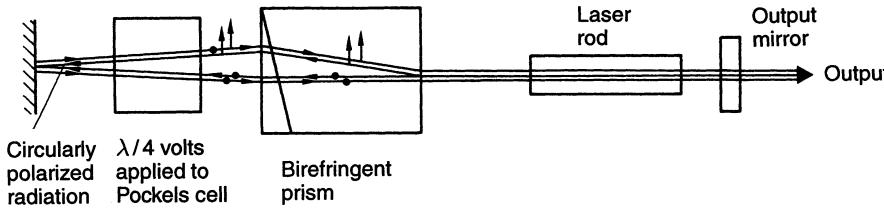

Fig. 8.17. Polarization insensitive Q-switch based on angular separation of orthogonally polarized beams [8.34]

A design which exploits directional differences between the two orthogonal beam components after passing through a birefringent prism has been proposed in [8.34]. A schematic diagram of the laser is shown in Fig. 8.17. The resonator contains a birefringent prism that replaces the linear polarizer commonly used in Q-switched lasers. After passing through the birefringent prism, radiation is split up into two orthogonally polarized components, the extraordinary (e) and the ordinary (o) rays, that propagate in two slightly different directions. When these two rays are reflected by the back mirror, a further separation of the two rays will occur. In this case the losses in the cavity will be very high and laser action will be suppressed. However, if a quarter-wave voltage is applied to the Pockels cell, the e and o rays returning to the prism will be interchanged. In this case, the walk off occurring in the first pass will be canceled by an equal and opposite walk off during the return pass, hence the beam returning to the laser rod will have low losses, allowing a Q-switched pulse to develop.

A very common resonator in military systems is a polarization coupled design such as depicted in Fig. 8.18. The resonator typically contains one or two Porro prisms to take advantage of the alignment insensitivity of these components. If such a laser is operated at high average power, the depolarization caused by thermally induced birefringence will drastically distort the output beam profile. An output beam resembling a Maltese cross will be obtained from a thermally stressed laser rod. However, in such a resonator, a birefringence compensation technique is possible by adding to the Porro prism a waveplate with the proper phase retardation and orientation.

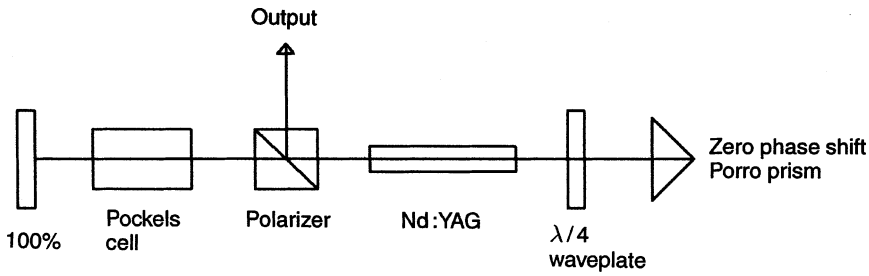

Fig. 8.18. Polarization output coupled resonator with birefringence compensation

Like the compensation with a Faraday rotator between the rear mirror and laser rod, or the placement of a 90° rotator between two laser rods, this technique relies on the fact that two passes occur in the thermally stressed laser rod before the beam is passed through the linear polarizer. However, there is a difference with regard to the above mentioned techniques. The phase difference between radial and tangential rays caused by birefringence is not cancelled by two passes of each ray through the same region of the laser rod, but by passing through two different, but symmetrically located points in each half of the rod. Each half being defined by the Porro prism bisecting plane. If the prism is oriented with its roof edge bisecting the rod axis, then each ray passing through one part in the rod returns at the opposite side of the bisecting plane through a section which is symmetrically opposite and at the same radial distance from the rod center. In a uniformly pumped laser rod, birefringence is radially symmetric and the amount of phase distortion depends only on the radius.

By changing the polarization state of the beam between the two passes, it is possible to cancel the relative phase difference between the tangential and radial components of polarization that occur in the first pass with equal and opposite phase changes in the return pass. The appropriate change of polarization between the two passes can be accomplished with a waveplate or optical rotator in front of the Porro prism [8.35, 36]. For example, the combination of a zero-phase-shift Porro prism and a quarter-waveplate with an orientation of 45° between its fast axis and the prism apex can accomplish this task. Any thermally induced depolarization effects that occur in the first pass are removed in the return path.

A Porro prism with zero phase shift (Fig. 8.18) is not a common optical component. As has been explained in Sect. 5.1.9. Porro prisms introduce a phase shift to a linearly polarized beam which depends on the refractive index and the angle between the plane of polarization and the roof edge. A Porro prism which does not introduce a phase shift requires dielectric coatings on the totally reflecting prism surfaces. Another combination, which results in a cancellation of the thermally induced depolarization, is a half-waveplate and a π-shift Porro prism at a relative orientation of 22.5°. Again the Porro prism requires dielectric coatings on the internally reflecting surfaces. The combination of a quarter- or half-waveplate and a Porro prism are only special cases of many possible combinations. They are of interest because these waveplates are readily available; however, the use of either of these waveplates requires a specially dielectrically coated Porro prism. By use of the Jones matrix method, a waveplate with a suitable phase change and orientation can be found for any uncoated Porro prism in order to achieve birefringence compensation. In [8.35, 36] curves are provided for waveplate-phase angle and Porro prism refractive index combinations, which permit the compensation of thermally induced depolarization in a laser rod.

The output coupling of the resonator, depicted in Fig. 8.18, can be optimized by a rotation of the Porro prism/waveplate combination while maintaining the relative angular position between these two components. As already mentioned, a change of the angle between the plane of polarization and the roof edge introduces a phase change in the return beam. However, in most situations it is found that it is more convenient to add a second waveplate to the resonator for control of the output coupling. Also, the 100% mirror shown in Fig. 8.18 can be replaced by a second Porro prism to add

alignment stability in two directions. In addition, space constraints drive the design very often to a folded configuration, shown, for example in Fig. 5.30.

8.3.5 Drivers for Electro-Optic Q-Switches

Switching a Pockels cell to obtain a quarter-wave retardation has the advantage that it requires only half the voltage of a half-wave retardation device. But the voltage has to be applied to the crystal for the duration of the pump pulse (i.e., about 240 μs for Nd:YAG). In the case of a half-wave retardation, the voltage is applied to the crystal only during the pulse build-up time at the end of the pump cycle (typically about 100 ns). As far as the electronics is concerned, for $\lambda/4$ switching a fast turn-off of the high voltage is critical and, for $\lambda/2$ switching a fast rise-time of the high voltage pulse is important to minimize resonator losses.

Operation of an electro-optically Q-switched laser requires fast switching of voltages in the multi-kilovolt regime. The driver for the Pockels cell must be a high-speed, high-voltage switch that also must deliver a sizeable current. The cell has a few tens of picofarads capacitance which is charged (or discharged) to several kilovolts in a few nanoseconds. The resulting current is of the order of 10–20 A. Common switching techniques include the use of MOSFETs, SCRs, and avalanche transistors.

A typical circuit is based on a Marx bank, in which a number of capacitors are charged in parallel and then connected in series by means of semiconductor switches. The advantage of the Marx bank circuit is that the voltage requirement of the power supply is only a fraction of the voltage generated at the crystal. Figure 8.19 illustrates such a design. The capacitors C_1 to C_n are all charged through resistors R_1 and R_n to about 1 kV. A string of transistors is connected in parallel to each capacitor and associated diode D. The transistors are operated close to their avalanche breakdown voltage. As soon as one transistor is triggered, all the transistors are switched on, which connects all capacitors in series and a large negative voltage appears on the Pockels cell. Typically four to six strings of avalanche transistors are employed to generate voltages in the 2.5–6 kV range starting with 0.8–1kV at the power supply.

The circuit illustrated in Fig. 8.19 is typical for producing a half-way voltage in the Pockels cell. In this case the high voltage is applied for only a very short time at the end of the pump cycle. If a high voltage power supply is available, a Marx bank is not needed and the switching circuit is simplified. Figure 8.20 shows a string of avalanche transistors (Q1–Q10) that will switch a high voltage applied to the Pockels cell quickly to zero. This circuit is intended for quarter wave operation of the Q-switch.

8.4 Acousto-Optic Q-Switches

In acousto-optic Q-switches, an ultrasonic wave is launched into a block of transparent optical material, usually fused silica. By switching on the acoustic field, a fraction of the energy of the main beam is diffracted out of the resonator, thus introducing a

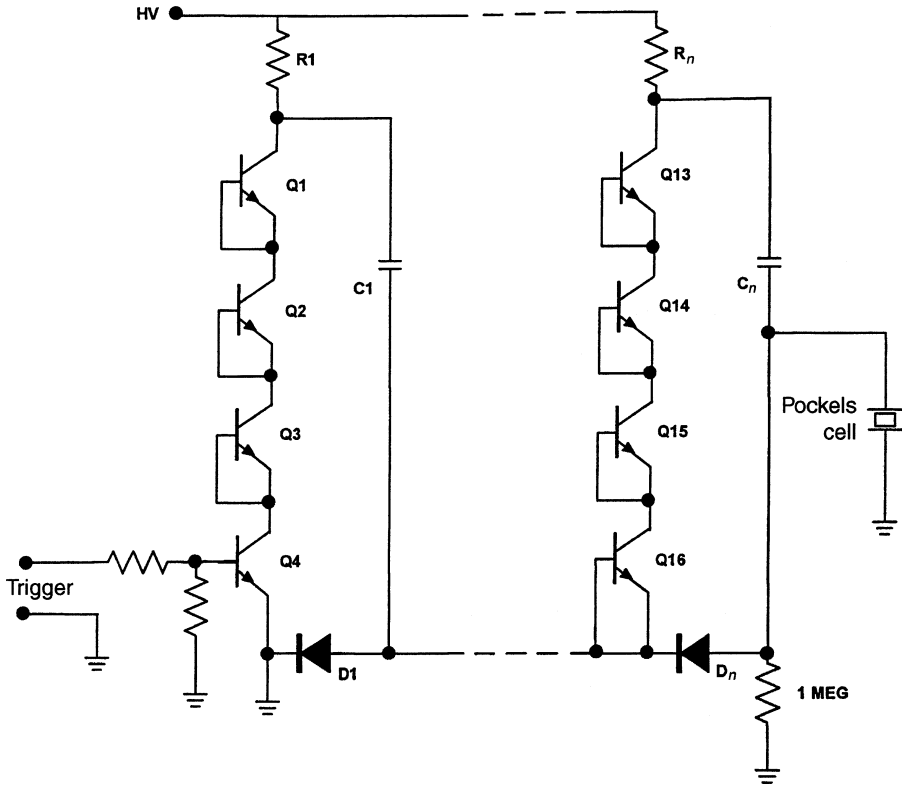

Fig. 8.19. Circuit diagram of Pockels cell drive electronics employing avalanche transistors

loss mechanism that prevents laser action. When the acoustic field is switched off, full transmission through the Q-switch cell is restored and a laser pulse is created.

The acousto-optic Q-switch is the device of choice for repetitively Q-switching cw lasers. The low-gain characteristics of cw-pumped solid-state lasers do not require very high extinction ratios, but do demand an exceptionally low insertion loss. Since high optical quality fused silica with antireflection coatings can be used as the active medium in the acousto-optical Q-switch, the overall insertion loss of the inactive Q-switch can be reduced to less than 0.5% per pass. The low-insertion loss of the acousto-optic Q-switch offers the convenience of converting from Q-switched to cw operation simply by removing the RF drive power.

An acousto-optic Q-switch is activated by the application of RF power to a transducer that is attached to the transparent medium. The resulting acoustic wave gives rise to a sinusoidal modulation of the density of the medium. The index of refraction is coupled to these periodic variations of the density and strain via the photoelastic effect. Considering only the one-dimensional case for an acoustic wave traveling in the y direction, we can write

$$n(y, t) = n_0 + \Delta n_0 \sin(w_s t - k_s y), \tag{8.28}$$

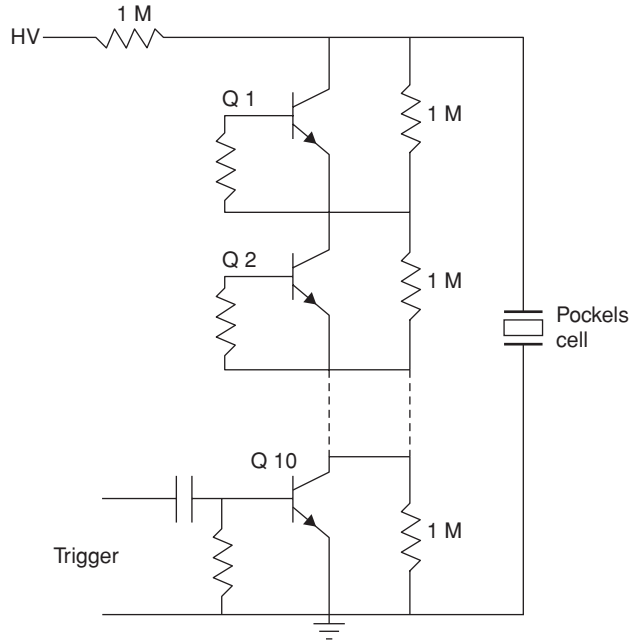

Fig. 8.20. Quarter–wave switching circuit for a Pockels cell

where n_0 is the average refractive index of the medium, Δn_0 is the amplitude of the index change, and $w_s = 2\pi\nu_s$ and $k_s = 2\pi/\lambda_s$ are the angular frequency and the wave vector of the sound wave which travels with the sound velocity $v_s = \nu_s\lambda_s$ through the medium.

8.4.1 Bragg Reflection

The refractive index change described by (8.28) forms a traveling-wave phase grating across the width of the optical beam. The grating has a period equal to the acoustic wavelength and an amplitude proportional to the sound amplitude. A portion of the optical beam which passes through the region occupied by the acoustic wave is diffracted by this phase grating. Acousto-optic Q-switches are operated at ultrasonic frequencies in the tens of megahertz, and the beam interaction length is on the order of several centimeters. In this so-called Bragg regime, the grating acts as a thick phase grating. The diffracted beam is primarily confined to a single direction and has a maximum at the Bragg angle. The condition for Bragg scattering to occur is $l\lambda \gg \lambda_s^2$, where l is the interaction length and λ and λ_s are the optical and acoustical wavelengths in the medium, respectively.

In the case of a short interaction length or long acoustical wavelength the acousto-optic cell becomes a thin phase grating and the light beam is diffracted into many orders. This is the regime of Raman–Nath scattering. Because of the higher RF power requirements, acousto-optic Q-switches are not used in this regime.

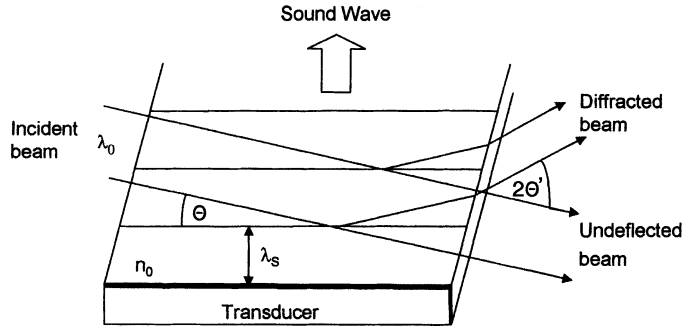

Fig. 8.21. Geometry for Bragg reflection

Figure 8.21 displays the geometry for Bragg reflection. The incident beam appears to be reflected from the acoustic wavefronts as if they were mirrors. This phenomenon is called acoustic Bragg reflection in analogy to the selective reflection of X-rays by the lattice of crystals first observed by Bragg. Conservation of energy and momentum of the photon–phonon interaction leads to the condition

$$\sin\Theta = \lambda/2\lambda_s, \tag{8.29}$$

where Θ is the angle of incidence between the optical beam and the acoustic wave, and $\lambda = \lambda_0/n_0$ is the optical wavelength in the diffracting medium. We can derive the Bragg condition (8.29) with the aid of Fig. 8.22 if we assume for the moment that there is no motion of the sound wave. Rays A and B are reflected by two successive acoustic wavefronts. The rays differ in pathlength by the distance $2s$. In order for the rays to be in phase and reinforce we require $2s = \lambda$. From Fig. 8.22 we also obtain the relationship $\sin\Theta = s/\lambda_s$. Elimination of s in these two equations yields the Bragg condition. The beam observed at the Bragg angle arrives from reflections at successive acoustic wavefronts. The rays from each wavefront add in phase and the total intensity is, therefore, N times the intensity of a single reflection.

The difference in direction of the diffracted and incident beam inside the medium is twice the Bragg angle, that is, $2\sin\theta$ or 2θ, since the angle is very small. Reflection at the external boundary of the device will increase the angle by n_0, accordingly we obtain

$$2\Theta' = \lambda_0/\lambda_s. \tag{8.30}$$

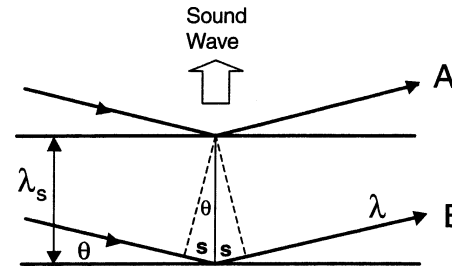

Fig. 8.22. Reflection of rays A and B by two successive acoustic wavefronts

The external angular separation of the two beams is equal in radians to the ratio of the optical to acoustic wavelengths.

A typical acousto-optic Q-switch uses fused silica as the ultrasonic medium and an RF frequency to the transducer for launching an acoustic wave of $\nu_s = 50$ MHz. The velocity of sound in fused silica is $v_s = 5.95$ km/s. With these numbers and $\lambda_0 = 1.06$ μm, we obtain $\lambda_s = 119$ μm and $2\theta' = 8.9$ mr.

Although of no particular consequence for Q-switch operation, it is worth mentioning that the diffracted beam is frequency shifted. The diffracted beam may be thought of as having been Doppler-shifted during diffraction from the acoustic traveling wave. It has the frequency $(\nu \pm \nu_s)$ depending on whether the optical beam is incident in front of the oncoming acoustic wave (see Fig. 8.21) or from behind the receding wave.

We will now calculate the partitioning of the power between the incoming and diffracted beam as a function of acoustic power and material parameters. A rigorous treatment of the subject that requires the solution of two coupled traveling wave equations can be found in [8.37, 38].

The total electric field $E(x, t)$ is taken as the sum of two waves along the distance x. The diffracted wave grows at a rate [8.39]

$$\frac{dE_1(x)}{dx} = \frac{1}{2}E_2\frac{d\varphi}{dx} \tag{8.31}$$

and the undeflected beam decreases at a corresponding rate

$$\frac{dE_2(x)}{dx} = -\frac{1}{2}E_1\frac{d\varphi}{dx}, \tag{8.32}$$

where E_1 and E_2 are the electric field strength of the diffracted and undeflected beam, respectively, and $d\varphi$ is the phase excursion of the beam over an incremental length x given by

$$d\varphi = \beta_0\frac{\Delta n_0}{n_0}dx, \tag{8.33}$$

where β_0 is the propagation constant $\beta_0 = 2\pi/\lambda_0$ in free space. Equations (8.31) and (8.32) have the solution

$$E_1 = E_3 \sin(\Delta\varphi/2) \tag{8.34}$$

and

$$E_2 = E_3 \cos(\Delta\varphi/2), \tag{8.35}$$

where E_3 is the amplitude of the wave entering the crystal.

The diffracted power P_1 as a function of the incident power P_3 follows from (8.34)

$$P_1/P_3 = \sin^2(\Delta\varphi/2) \tag{8.36}$$

and the reduction of power of the undeflected beam is obtained from (8.35)

$$P_2/P_3 = \cos^2(\Delta\varphi/2), \tag{8.37}$$

where $\Delta\varphi$ is the total phase shift the beam experienced over the interaction length l,

$$\Delta\varphi = l\beta_0\Delta n_0. \tag{8.38}$$

The sum of the powers of the undeflected and diffracted beams remains constant $P_1 + P_2 = P_3$. Now we have to connect a change of Δn_0 with the acoustic power P_{ac} in the medium.

The change of refractive index as a function of strain s is given by [8.18]

$$\Delta n_0 = \frac{n_0^3 p_{ij}}{2} s, \tag{8.39}$$

where p_{ij} is the elasto-optic coefficient in the medium, and the strain s is related to the acoustic power P_{ac} by [8.37]

$$s = \left[\frac{2P_{\text{ac}}}{\rho_0 v_s^3 l w}\right]^{1/2}. \tag{8.40}$$

In the above equation v_s is the velocity of sound in the medium, ρ_0 is the mass density, and l and w are the length and width of the transducer that launches the acoustic wave into the medium. Introducing (8.38–40) into (8.36) yields

$$\frac{P_1}{P_3} = \sin^2\left[\frac{\pi}{\lambda}\left(\frac{l P_{\text{ac}} M_{\text{ac}}}{2w}\right)^{1/2}\right]. \tag{8.41}$$

The quantity M_{ac} is a material constant that determines the inherent efficiency of diffraction and is called the figure of merit

$$M_{\text{ac}} = n_0^6 p_{ij}^2/\rho_0 v_{\text{s}}^3. \tag{8.42}$$

It is apparent from (8.41) that the amount of diffracted power depends on the material parameters expressed by M_{ac}, the ratio of length to width of the interaction path and the acoustical power P_{ac}. In a given material, for example fused silica, the value of the photoelastic coefficient p_{ij} in (8.42) depends on the plane of polarization of the light beam with respect to the ultrasonic propagation direction and on the type of ultrasonic wave, that is, longitudinal or shear wave. With shear wave generation the particle motion is transverse to the direction of the acoustic wave propagation direction. In this case the dynamic optical loss is independent of polarization in isotropic materials such as fused quartz.

Table 8.2 lists the pertinent material parameters for an acousto-optic Q-switch fabricated from fused silica. The p coefficients and velocity of sound in fused silica are from [8.40, 41]. The figure of merit M_{ac} follows from (8.42) with $n_0 = 1.45$ at 1.06 μm and $\rho_0 = 2.2$ g/cm^3. The acoustic power requirement for 1% diffraction has been calculated from (8.41) for $l/w = 10$ and $\lambda = 1.06$ μm. The dimension of P_{ac} in (8.41) is erg/s (1 erg/s $= 10^{-7}$ W).

8.4.2 Device Characteristics

Figure 8.23 shows an optical schematic of a cw-pumped laser that contains an acousto-optic Q-switch. The Q-switch consists of a fused silica block to which a crystalline

Table 8.2. Material parameters of acousto-optic Q-switches employing fused silica

Acoustic wave	p Coefficient	Polarization of optical beam with respect to acoustic wave vector	Velocity of sound $\times 10^5$ (cm/s)	Figure of merit M_{ac} $\times 10^{-18}$ (s^3/g)	Acoustical power P_{ac}(W) for 1% diffraction ($l/w = 10$)
Shear wave	$p_{44} = 0.075$	Independent	3.76	0.45	0.51
Longitudinal	$p_{11} = 0.121$	Parallel	5.95	0.30	0.77
Longitudinal	$p_{12} = 0.270$	Perpendicular	5.95	1.46	0.16

quartz or an $LiNbO_3$ transducer is bonded. Both the transducer and the fused silica interface contain vacuum-deposited electrodes to allow for electrical connections. An inductive impedance-matching network couples the signal of the RF generator to the quartz transducer. The ultrasonic wave is launched into the Q-switch block by the piezoelectric transducer that converts electrical energy into ultrasonic energy. The laser is returned to the high Q-state by switching off the driving voltage to the transducer. With no ultrasonic wave propagating through it, the fused silica block returns to its usual state of high optical transmission and a Q-switch pulse is emitted. The width of the transducer is typically 3 mm, which is about twice the beam diameter for most TEM_{00}-mode Nd:YAG lasers. The length of the Bragg cell and the transducer is around 50 mm. From (8.41) it follows that a large length-to-width ratio reduces the acoustic power requirement for a given diffraction ratio P_1/P_3.

Virtually all acousto-optic Q-switches are single-pass devices, i.e., the acoustic wave generated by the transducer is absorbed after traveling across the interaction region. The absorber, consisting of a piece of lead attached to the tapered end of the

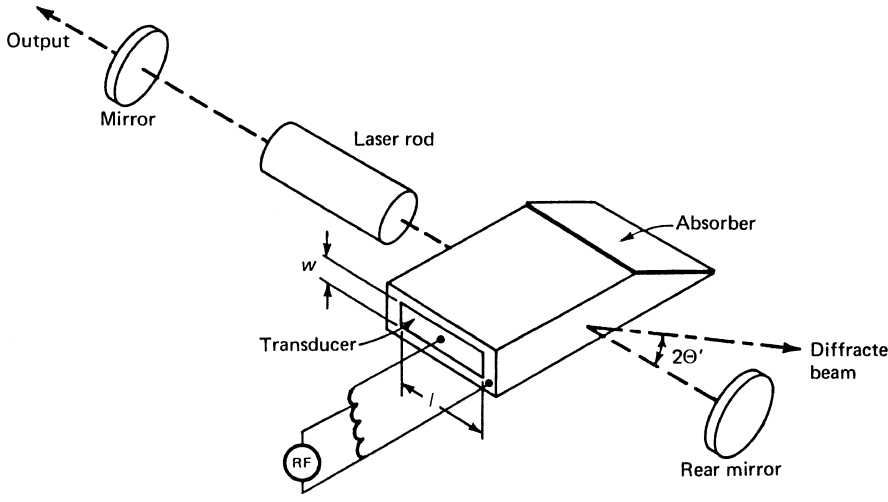

Fig. 8.23. Acousto-optic Q-switch employed in a cw-pumped Nd:YAG laser

quartz block, prevents reflected acoustical waves from interfering with the incident light beam.

Although the figure of merit M_{ac} of fused quartz is quite low, its optical high-quality, low optical absorption, and high damage threshold make it superior to other, more efficient acousto-optic materials, such as lithium niobate ($LiNbO_3$), lead molybdate ($PbMoO_4$), tellurium dioxide (TeO_2), and dense flint glass. These materials are usually employed in low-power light modulators and optical scanners.

By properly choosing the parameters of the acousto-optic device, a large enough fraction of the laser beam can be deflected out of the resonator to provide an energy loss that inhibits laser action. The frequency of the RF generator determines the diffraction angle according to (8.30), whereas the magnitude of the diffracted power is controlled by the RF power according to (8.41). The frequency of the RF signal driving the transducer is typically in the 40–50 MHz range. For these frequencies we obtain, with the values from Table 8.2 for both shear wave and longitudinal wave Q-switches, scattering angles in fused quartz between 14.1 and 7.1 mr. These angles are large enough to deflect the diffracted beam out of the resonator.

The amount of acoustical power required to achieve a certain diffraction efficiency can be calculated from (8.41). Unpolarized lasers are usually Q-switched with shear-wave devices, whereas for polarized laser radiation longitudinal modulators are employed. A longitudinal Q-switch in which the large p_{12} coefficient is utilized requires substantially lower RF powers compared to a shear wave device.

For the practical case of a shear wave Bragg cell having a length of $l = 50$ mm and a width of $w = 3$ mm, we find from (8.41) that in order to deflect 35% of the laser beam out of the resonator an acoustic power of 11.7 W is required. Since the Q-switch diffracts radiation in both directions the total insertion loss per round trip is $\delta = (P_1/P_3)(2 - P_1/P_3)$, where (P_1/P_3) is the fraction of radiation diffracted out of the resonator in one pass. For the example above, one obtains a round trip insertion loss of 58%, which is large enough to prevent laser action in most cw lasers. The conversion efficiency of RF power delivered to the transducer to acoustic power is on the order of 25–30%; therefore, at least 40 W of RF power have to be delivered to the transducer. If the laser output is polarized, a Bragg cell with a longitudinal wave can be utilized, and in this case only 12 W of RF power is required to achieve the same insertion loss.

The Q-switch must be able to switch from the high-loss to the low-loss state in less than the time required for the laser pulse to build up if maximum output energy is to be achieved. The turn-off time of an acousto-optical Q-switch is determined by the transit time of the sound wave across the beam diameter. Depending on the type of interaction, the transit time of the acoustic wave across a 1-mm diameter beam is between 266 and 168 ns. The relatively slow transit-time is not a serious drawback since the Q-switch pulse evolution time in most cw-pumped systems is considerably larger. Performance of an acousto-optic Q-switched, cw-pumped Nd:YAG laser is shown in Fig. 8.8. An acousto-optic Q-switch allows laser operation with a continuously adjustable pulse repetition rate, shown is the range from 100 Hz to about 40 KHz.

As already mentioned, an acousto-optic device is the most widely used Q-switch for cw-pumped Nd lasers. From (8.41) it follows that the modulation depth is inversely

proportional to the wavelength. Therefore, for longer wavelengths the modulation depth decreases, which has to be compensated for by a drastic increase in acoustic drive power since modulation depth increases only with the square root of P_{ac}. This makes the use of acousto-optic devices difficult for Q-switching mid-infrared lasers. In [8.42] an acousto-optic Q-switched Er:YSGG laser with an output at 2.79 μm and which uses a TeO_2 crystal as the interaction medium, is described.

Despite these difficulties several erbium lasers have been Q-switched with acousto-optic Q-switches. By using a linearly polarized beam for maximum diffraction efficiency and TeO_2 as the Q-switch medium, an efficient acousto-optic Q-switch for a Er:YSGG laser at 2.79 μm has been reported in [8.42]. Pulse energies of 27 mJ with durations of 125 ns have been obtained from a 90-mm-long and 4-mm-diameter rod. Linear polarization was achieved with a Si plate orientated at Brewster angle.

8.5 Passive Q-Switches

A passive Q-switch consists of an optical element, such as a cell filled with organic dye or a doped crystal, which has a transmission characteristic as shown in Fig. 8.24 The material becomes more transparent as the fluence increases, and at high fluence levels the material "saturates" or "bleaches," resulting in a high transmission. The bleaching process in a saturable absorber is based on saturation of a spectral transition. If such a material with high absorption at the laser wavelength is placed inside the laser resonator, it will initially prevent laser oscillation. As the gain increases during a pump pulse and exceeds the round-trip losses, the intracavity power density increases dramatically causing the passive Q-switch to saturate. Under this condition the losses are low and a Q-switch pulse builds up.

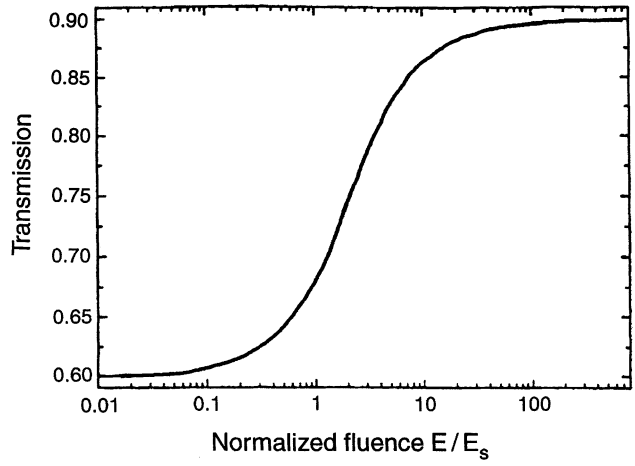

Fig. 8.24. Nonlinear transmission of a saturable absorber versus fluence normalized to the saturation fluence E_s of the absorber

Since the passive Q-switch is switched by the laser radiation itself, it requires no high voltage, fast electro-optic driver, or RF generator. As an alternative to active methods, the passive Q-switch offers the advantage of an exceptional simple design, which leads to very small, robust, and low-cost systems. The major drawbacks of a passive Q-switch are the lack of a precision external trigger capability and a lower output compared to electro-optic or acousto-optic Q-switched lasers. The latter is due to the residual absorption of the saturated passive Q-switch which represents a rather high insertion loss.

Originally, saturable absorbers were based on different organic dyes, either dissolved in an organic solution or impregnated in thin films of cellulose acetate. The poor durability of dye-cell Q-switches, caused by the degradation of the light sensitive organic dye, and the low thermal limits of plastic materials severely restricted the applications of passive Q-switches in the past. The emergence of crystals doped with absorbing ions or containing color centers has greatly improved the durability and reliability of passive Q-switches.

The first new material to appear was the F_2^-:LiF color center crystal. The color centers are induced in the crystal by irradiation with gamma, electron, or neutron sources. Today, the most common material employed as a passive Q-switch is Cr^{4+}: YAG. The Cr^{4+} ions provide the high absorption cross section of the laser wavelength and the YAG crystal provides the desirable chemical, thermal, and mechanical properties required for long life.

A material exhibiting saturable absorption can be represented by a simple energy-level scheme such as that shown in Fig. 8.25. For the moment we will consider only levels 1–3. Absorption at the wavelength of interest occurs at the 1–3 transition. We assume that the 3–2 transition is fast. For a material to be suitable as a passive Q-switch, the ground-state absorption cross section has to be large and, simultaneously, the upper state lifetime (level 2) has to be long enough to enable considerable depletion of the ground state by the laser radiation. When the absorber is inserted into the laser cavity, it will look opaque to the laser radiation until the photon flux is large enough to depopulate the ground level. If the upper state is sufficiently populated the absorber

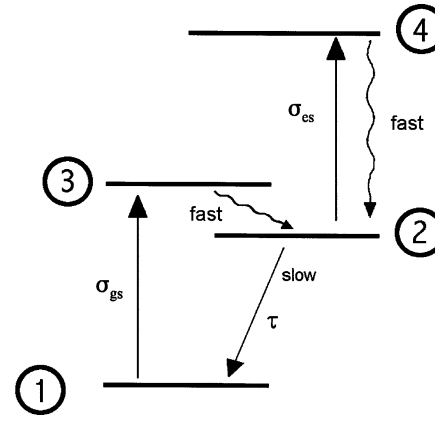

Fig. 8.25. Energy levels of a saturable absorber with excited-state absorption (σ_{gs} and σ_{es} are the ground-state and excited-state absorption cross sections, respectively, and τ is the upper state lifetime)

becomes transparent to the laser radiation, a situation that is similar to a three-level laser material pumped to a zero inversion level.

Solutions of the rate equation lead to an absorption coefficient which is intensity dependent [8.43]

$$\alpha_0(E) = \frac{\alpha_0}{1 + E_\mathrm{i}/E_\mathrm{s}}, \tag{8.43}$$

where α_0 is the small-signal absorption coefficient and E_s is a saturation fluence

$$E_\mathrm{s} = h\nu/\sigma_\mathrm{gs}, \tag{8.44}$$

where σ_gs is the absorption cross section for the 1–3 transition.

Important characteristics of a saturable absorber are the initial transmission T_0, the fluence E_s at which saturation becomes appreciable, and the residual absorption which results in a T_max of the fully bleached absorber.

The small signal transmission of the absorber is

$$T_0 = \exp(-\alpha_0 l_\mathrm{s}) = \exp(-n_\mathrm{g}\sigma_\mathrm{gs} l_\mathrm{s}), \tag{8.45}$$

where l_s is the thickness of the bleachable crystal and n_g is the ground state density. In order to calculate the transmission as a function of fluence, the photon flux and population density must be considered as a function of position within the absorbing medium.

Similar to the situation which occurs in pulse amplifiers (Sect. 4.1), differential equations for the population density and photon flux have to be solved. The solution is the Frantz–Nodvik equation, which is identical to (4.11) except that gain G, G_0 is replaced by transmission T_i, T_0. Therefore, the energy transmission T_i of an ideal saturable absorber as a function of input fluence E_i is given by

$$T_\mathrm{i} = \frac{E_\mathrm{s}}{E_\mathrm{i}} \ln[1 + (e^{E_\mathrm{i}/E_\mathrm{s}} - 1)T_0]. \tag{8.46}$$

Equation (8.46) reduces to $T_\mathrm{i} = T_0$, for $E_\mathrm{i} < E_\mathrm{s}$, and $T_\mathrm{i} = 1$, for $E_\mathrm{i} > E_\mathrm{s}$.

In practical saturable absorbers, the transmission never reaches 100%; the reason being photon absorption by the excited atoms. A passive Q-switch requires a material which exhibits saturation of the ground-state absorption. However, most materials also exhibit absorption from an excited state. This is illustrated in Fig. 8.25 by the transition from the upper state (level 2) to some higher level 4 which has an energy level corresponding to the laser transition. As the ground state is depleted, absorption takes place increasingly between levels 2 and 4. Excited-state absorption (ESA) results in a residual loss in the resonator when the ground-state absorption has been saturated. The 2–4 transition does not saturate because of the fast relaxation of level 4. A saturable absorber is useful for Q-switching only as long as $\sigma_\mathrm{gs} > \sigma_\mathrm{es}$, where σ_es is the cross section for ESA.

A saturable absorber with ESA can be described by a four-level model [8.43, 44]. In this case, maximum transmission $T_{\max}$ is given by

$$T_{\max} = \exp(-n_g \sigma_{es} l_s). \tag{8.47}$$

In [8.44] an approximation in closed form, which gives the shape of the transmission versus fluence curve in the presence of ESA, has been derived. For a nonideal absorber the transmission T_n can be approximated by

$$T_n = T_0 + \frac{T_i - T_0}{1 - T_0}(T_{\max} - T_0), \tag{8.48}$$

where T_i is the transmission of an ideal absorber given by (8.46) and T_0 and $T_{\max}$ are the lower and upper limits of the transmission.

In Fig. 8.24, T_n is plotted for the case of $T_0 = 60\%$ and $T_{\max} = 90\%$. For a given saturable absorber one needs to know the cross sections σ_{gs} and σ_{es}, the ground-state concentration n_g, and the thickness l_s of the material. With these quantities known one can calculate T_0, $T_{\max}$, and E_s and plot a transmission versus energy density curve as determined by (8.48).

Because of the importance of Cr^{4+}:YAG as a passive Q-switch material, we will briefly review the properties of this material. In order to produce Cr^{4+}:YAG, a small fraction of chromium ions in YAG are induced to change valence from the normal Cr^{3+} to Cr^{4+} with the addition of charge compensating impurities such as Mg^{2+} or Ca^{2+}. The crystal Cr^{4+}: YAG has broad absorption bands centered at 410, 480, 640, and 1050 nm. Published values for the cross section of the ground state vary greatly [8.44, 45]. The most recent measurements indicate $\sigma_{gs} = 7 \times 10^{-18}$ cm^2 and $\sigma_{es} = 2 \times 10^{-18}$ cm^2 for the excited-state absorption at the Nd:YAG wavelength [8.44]. The excited-state lifetime(level 2 in Fig. 8.25) is 4.1 μs and the lifetime of the higher excited state (level 4) is 0.5 ns. With $h\nu = 1.87 \times 10^{-19}$ J at 1.06 μm and the above value for σ_{gs} one obtains a saturation fluence of $E_s = 27$ mJ/cm^2 for Cr^{4+}:YAG.

Commercially available Cr^{4+}:YAG passive Q-switches are specified by the low-power transmission at the laser wavelength. Typical transmission values range from 30 to 50%, and the crystal thickness is usually between 1 and 5 mm. Values of the small signal absorption coefficient α_0 vary from 3 to 6 cm^{-1}. For example, for $\alpha_0 = 4$ cm^{-1} and $l_s = 2$ mm the low-power transmission is $T_0 = 45\%$.

Figure 8.26 illustrates the transmission of a 2.65-mm-thick sample of Cr^{4+}: YAG. The transmission starts at about $T_0 = 53.5\%$ for low power, increases linearly, and then saturates at about $T_{\max} = 84\%$ for high fluence [8.46]. From (8.45) follows a Cr^{4+} ion density of $n_g = 3.4 \times 10^{17}$ cm^{-3} for this sample.

For a given pump power, i.e. gain in the laser medium, there is an optimal choice of output coupler reflectivity and unsaturated absorber transmission. A design procedure that permits the optimization of a passively Q-switched laser has been developed by Degnan [8.47] by applying the Lagrange multiplier method in analogy to his analysis of actively Q-switched lasers. Figure 8.27, which is adapted from [8.47], shows that the design procedure permits the optimum choice of the unsaturated

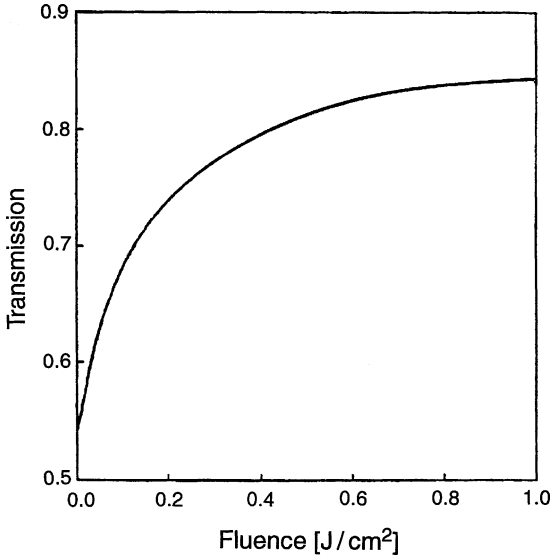

Fig. 8.26. Transmission versus fluence for a 2.65-mm-thick Cr^{4+}:YAG absorber [8.46]

Q-switch transmission T_0 and the output mirror reflectivity R for a given gain G_0. The above quantities are normalized as follows:

$$x = \frac{1}{\delta} \ln\left(\frac{1}{R}\right) \qquad y = \frac{-\ln T_0}{\ln G_0} \qquad z = \frac{\ln G_0^2}{\delta}, \tag{8.49}$$

where

$$\delta = \delta_R + 2\sigma_{es}\, n_g\, l_s. \tag{8.50}$$

The terms in (8.50) are the combined roundtrip loss in the resonator caused by dissipative losses δ_R and the residual absorption in the fully saturated Q-switch.

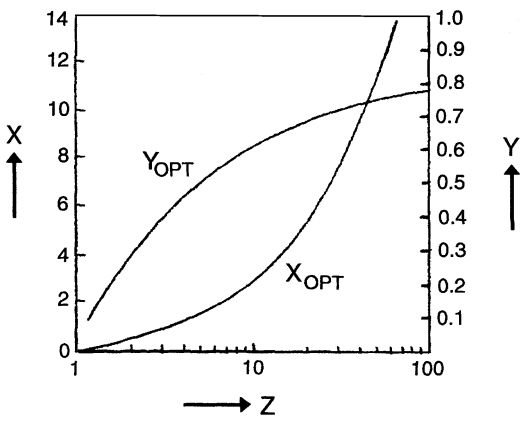

Fig. 8.27. Dependence of the optimum mirror reflectivity x and absorber transmission y on laser gain z. All parameters are normalized according to (8.49)

The variable z is the same that has been used in the analysis of the actively Q-switched case (see Eq. (8.8).

The optimization of a passively Q-switched laser can proceed along the following path: First one determines the single pass, small-signal gain G_0, and optical losses δ_R according to the procedure outlined in Sect. 3.4.2. From the manufacturer data which usually provides the optical density of T_0 of the crystal, one can calculate n_g and therefore δ. With G_0 and δ known, the parameter z can be calculated and with it x_{opt} and y_{opt} follow from Fig. 8.27.

Rearranging (8.49) one obtains

$$R_{opt} = \exp(-x_{opt}\delta) \qquad T_{opt} = \exp(-y_{opt} \ln G_0). \tag{8.51}$$

Building upon the work reported in [8.47] the analysis of passive Q-switched lasers has been expanded to include ESA in the saturable absorber [8.48, 49].

Passive Q-switching of pulsed and cw-pumped Nd:lasers employing Cr^{4+}:YAG are described in [8.46, 48, 50–52]. In a passively Q-switched, cw-pumped laser, once a certain threshold is reached, peak power and pulse width do not change further, but the repetition rate increases approximately linearly with pump input power [8.53].

According to (8.11) the pulse width of a Q-switched laser is directly proportional to the cavity round trip time and therefore to the resonator length. Passive Q-switches permit the design of lasers with very short resonators because the Q-switch and laser crystal can be closely packaged. For example, diode-pumped microchip lasers have resonators typically less than 1 mm in length. These lasers, consisting of a Nd:YAG crystal bonded to a thin piece of Cr^{4+}:YAG and with reflective coatings applied to the outside surfaces, have produced Q-switch pulses well below a nanosecond [8.54–56].

For passive Q-switching of lasers other than Nd-doped crystals, particularly lasers emitting at 1.5 μm and 2 μm, different saturable absorbers are required. Passive Q-switching of erbium-doped lasers emitting at 1.5 μm has been achieved with CaF_2 [8.57, 58]. For passive Q-switching of 2-μm lasers, such as Tm:YAG or Tm:Cr:YAG lasers, the crystal Ho:YLF has been used as an effective saturable absorber [8.59].

In the passive Q-switches discussed so far, the *transmission* increases with intensity. A different kind of passive Q-switch is the semiconductor saturable absorber mirror. In such a mirror *reflectivity* increases with intensity. As will be explained in more detail in Sect. 9.2.4, a semiconductor saturable absorber consists of an InGaAs/GaAs multiple quantum well absorber layer with appropriate coatings applied to both surfaces. This device is mostly employed for passive mode-locking; however, it can also be used for passively Q-switching lasers.

The layout of a diode-pumped Nd:YVO_4 microchip laser containing a semiconductor saturable absorber mirror (SESAM) Q-switch is illustrated in Fig. 8.28. The 3% doped Nd:YVO_4 crystal, with a thickness of 200 μm and an absorption length of about 100 μm, is sandwiched between a 10% output coupler and the saturable absorber mirror. At an incident pump power of 460 mW pulses with a duration of 56 ps and a peak power of 1.1 kW were obtained. The pulse repetition rate was 85 kHz [8.60].

The compactness which can be achieved with a passive Q-switched laser is illustrated in the following example. For a space-borne high-resolution lidar system

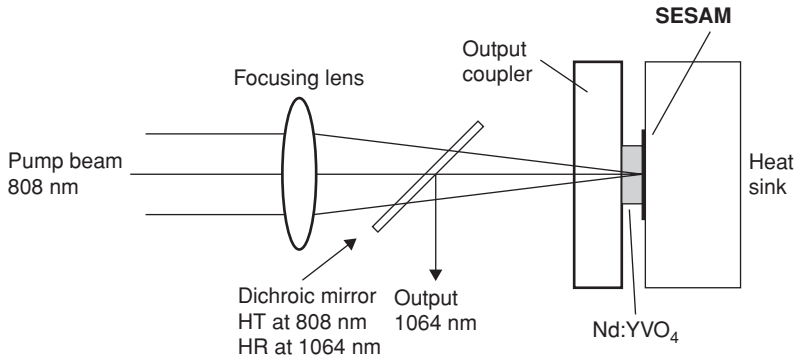

Fig. 8.28. Layout of a passively Q-switched Nd:YVO_4 microchip laser [8.60]

an extremely small, conduction-cooled laser transmitter was required having pulse width of less than 2 ns [8.52]. The optical layout is sketched in Fig. 8.29a. The laser uses a single 100 W quasi-cw diode bar to pump a ten bounce zigzag Nd:YAG slab of 13 mm length and 1×0.75 mm^2 cross-section.

The passive Q-switch permits the design of a resonator which is only a few centimeters in physical length. The optical length of the resonator comprising a flat and curved mirror is 6.75 cm, which results in a roundtrip time of $t_r = 0.45$ ns. The laser produces a TEM beam with an output energy of 0.85 mJ per pulse and a pulse length of 1.4 ns at a repetition rate of 100 Hz (see Fig. 8.29b). The pump radiation from the diode array is collimated with a cylindrical lens to confine the radiation into a 500-μm-wide region within the slab. With this arrangement a small pump mode volume can be realized which well overlaps the resonator fundamental mode. Pumping for 200 μs produces 20 mJ of pump power. The single pass, small-signal gain was measured to be about $G_0 = 8$. The AR-coated Cr^{4+}:YAG crystal has a thickness of 2 mm and an optical density of 0.5 or $T_0 = 0.32$ in the unsaturated state. With the value of T_0 and with σ_{gs} for Cr^{4+}:YAG, we can calculate the ground-state population density

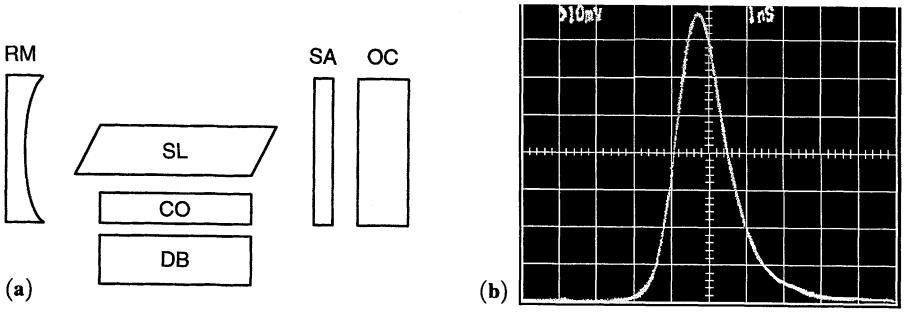

Fig. 8.29. (a) Optical schematic of a passively Q-switched Nd:YAG oscillator. SL, Nd:YAG slab; DB, diode bar; CO, coupling optics; OC, output coupler; RM, rear mirror; SA, saturable absorber. (b) Oscilloscope trace of the Q-switched output pulse (horizontal: 1 ns/div) [8.52]

n_g from (8.45). Introducing n_g and σ_{gs} into (8.47) gives the saturated transmission $T_{max} = 0.72$. This results in a roundtrip loss of about $\delta = 0.6$, if one includes 4% losses in the crystal slab. Typical of passive Q-switched lasers, the insertion loss is dominated by the residual absorption in the Q-switch caused by undepleted ground-state population density and excited-state absorption. As follows from (8.45) and (8.47), the ratio of excited-state to ground-state absorption cross section is fixed for a given saturable absorber $\ln T_{max}/\ln T_0 = \sigma_{es}/\sigma_{gs}$.

The output beam has a diameter of about 0.5 mm, which gives a fluence of 0.45 J/cm^2. Since the output coupler has a reflectivity of $R = 20\%$, the fluence within the saturable absorber is about 0.67 J/cm^2. This is 25 times above the saturation level for Cr^{4+}:YAG and according to the curves of Figs. 8.24 and 8.26, it is close to the maximum transmission for this material.

Generally, a good agreement is obtained between the calculated and measured values of pulse width, optimum mirror reflectivity, and Q-switch transmission. With the above values for G_0 and δ, one obtains $z = 6.9$ from (8.8). The pulse width calculated from (8.11) is 1.1 ns for this laser. This compares well with the measured pulse width of 1.4 ns. From (8.49) follows $x_{opt} = 2.0$ and $y_{opt} = 0.56$. The optimum values for unsaturated transmission and output coupler reflectivity are therefore $R_{opt} = 30\%$ and $T_{opt} = 31\%$.

The Cr^{4+}:YAG crystal selected for this laser had an optical density T_0 at the unsaturated state, which comes very close to the optimum predicted value. The reflectivity of the output mirror was deliberately chosen to be lower than the calculated value R_{opt}.

Energy output versus mirror reflectivity is not a strongly peaked function, and it is sometimes desirable to select a lower reflectivity for the output mirror rather than the optimum value in order to make the laser more robust from the point of view of optical damage and multiple pulsing. A lower reflectivity of the output coupler reduces the fluence in the cavity which reduces the likelihood of optical coating damage. Multiple Q-switched output pulses occur if the unsaturated transmission of the absorber and/or the output mirror reflectivity is too high. In this case, Q-switching occurs early in the pump pulse. With the proper values and ratio of output coupling to absorption in the Q-switch, a single pulse can be generated which should occur near the end of the pump pulse.

8.6 Cavity Dumping

A means for generating extremely short Q-switched laser pulses involves Q-switching the laser with 100% mirrors on both ends of the cavity and then, at the peak of the circulating power, rapidly switching the output mirror from 100 to 0% reflection. This leads to a rapid dumping of the entire optical energy from within the cavity. One of the advantages of this technique is the production of Q-switched pulses whose width is primarily a function of the oscillator cavity length, rather than the gain characteristics of the laser medium. Specifically, the laser pulse width at the half-power points will be equivalent to the roundtrip transit time in the cavity, with the

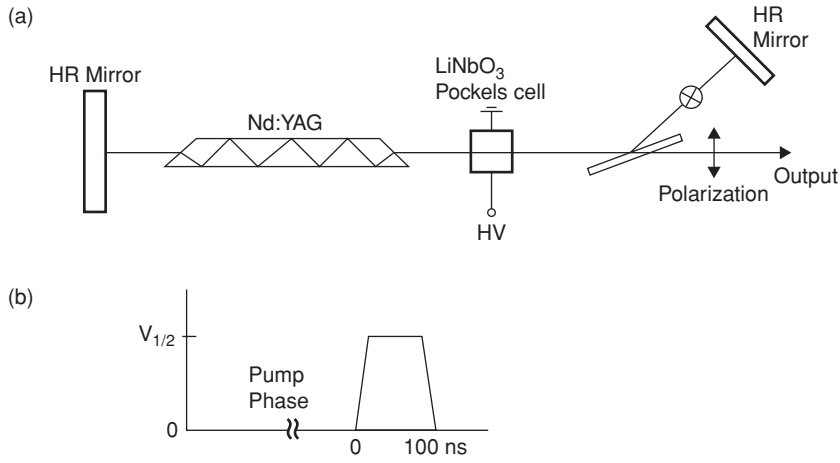

Fig. 8.30. (a) Optical schematic of a cavity dumped Nd:YAG laser and (b) voltage at the Pockels cell

condition that the Q-switch employed be switched within this same time period. Thus, based on typical cavity dimensions, pulse widths in the range of 2–5 ns are feasible for oscillators whose pulse widths are of the order of 10–20 ns in the normal Q-switch mode.

Figure 8.30 shows the layout of a Nd:YAG slab laser designed to generate short pulses by cavity dumping. During the 200-μs-long pump pulse, the horizontally polarized beam is transmitted by a thin film or calcite polarizer thereby preventing optical feedback. Upon reaching peak energy storage in the Nd:YAG crystal, the Pockels cell is biased to its half-wave retardation voltage. The vertically polarized radiation is now reflected by the polarizer to the high reflectivity mirror, and a high Q is established in the resonator.

When the power in the cavity reaches its peak value, the bias is removed from the Pockels cell in a time period of about 2 ns. The cavity energy then literally drains out of the cavity in the time required for the radiation to travel one round trip in the optical cavity. The combination of the polarizer, Pockels cell, and 100% mirror comprises what amounts to a high-speed voltage-variable mirror whose reflectivity is changed from 0 during the pumping cycle to 100% during the pulse buildup, and back to 0 during the cavity dumping phase.

Cavity dumping is also possible in a continuously pumped laser. As is the case for repetitively Q-switching, a continuous train of pulses is emitted. However, energy accumulation and storage between output pulses are primarily in the optical field for cavity dumping, and primarily in the population inversion for Q-switching.

The finite buildup time of the field inside the laser cavity and the time required to repump the inversion set an upper limit to the repetition rate available from Q-switched lasers. This maximum value of repetition rate for Q-switched Nd:YAG lasers is of the order of 50–100 kHz. Cavity dumping of continuously pumped lasers is a way

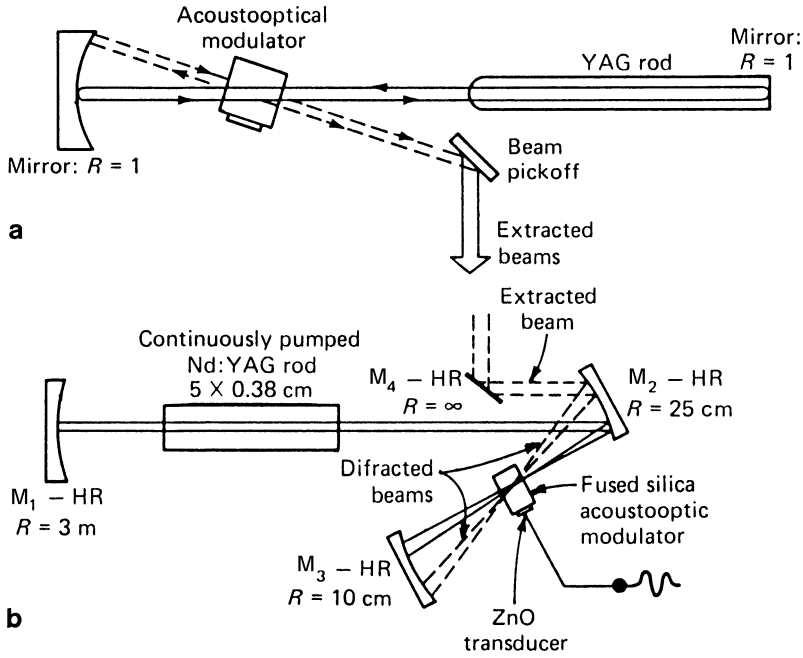

Fig. 8.31. Common arrangements for cavity dumping of cw-pumped solid-state lasers. The broken lines indicate the beams which are diffracted by the modulator

to obtain pulsed output at higher repetition rates than are available by Q-switching. Repetition rates from 125 kHz up to several megahertz for cavity dumping have been achieved with cw-pumped Nd:YAG lasers.

Figure 8.31 exhibits two common arrangements employed for cavity dumping of cw-pumped solid-state lasers [8.61, 62]. Essentially all systems of this type employ acousto-optic modulators as the switching element. In order to obtain fast switching action, the incident beam must be focused to a narrow waist inside the modulator. The two oscillator designs differ in the way the optical beam is focused into the modulator.

In Fig. 8.31a the modulator is located at a beam waist created by a concave mirror and by the thermal lens properties of the laser rod. The acoustic wave in the fused silica causes Bragg scattering of the forward- and backward-traveling light beam in the resonator. The two diffracted beams which are obtained from the cavity-dumped oscillator are initially traveling in opposite directions; therefore, their frequencies are shifted to a value of to $\omega + \Omega$ and $\omega - \Omega$, where ω is the frequency of the incident beam and Ω is the frequency of the acoustic wave. The two diffracted beams are extracted from the cavity as a single beam and deflected out of the system by a mirror. In Fig. 8.31b the cavity is formed by three high-reflectivity mirrors M_1, M_2, and M_3. The mirror curvature and the distance between M_2 and M_3 are chosen such that the light beam between M_2 and M_3 is focused to a small diameter at

the center of curvature of M_3. The modulator is inserted at the waist of the optical beam.

Acousto-optic modulators employed for cavity dumping differ from their counterparts used in Q-switch applications in several respects:

1) Compared to Q-switching, the cavity-dump mode requires much faster switching speeds. The rise time in an acousto-optic modulator is approximately given by the beam diameter divided by the velocity of the acoustic wave. In order to obtain rise times around 5 ns, a value which is required for efficient cavity dumping, the incident beam must be focused to a diameter of approximately 50 μm.
2) For efficient operation in the cavity-dump mode, it is important that essentially all the circulating power be diffracted into the first diffraction order. In a Bragg device the diffraction efficiency increases with the rf carrier frequency and therefore modulators employed in cavity dumpers operate at considerably higher frequencies, i.e., 200–500 MHz as compared to acousto-optic Q-switches.
3) In order to generate an output pulse in the cavity-dump mode, a short rf pulse is applied to the modulator, whereas in an acoustooptic Q-switch the rf carrier is turned off for the generation of an output pulse.
4) The cavity is never kept below threshold condition as in the Q-switched mode of operation. If the cavity is dumped of all its energy, the field has to build itself from the noise level. Repetitive cavity dumping was observed to become unstable in this case. If the repetition rate is lowered, the laser material is pumped higher above threshold between pulses and, therefore a larger fraction of the stored energy is extracted from the system (see Sect. 8.1). The lower limit of the dumping repetition rate is reached when the internal laser energy decreases to one photon immediately after dumping. The upper limit of the cavity dumping repetition rate is set by the switching speed of the modulator. Repetition rates as high as 10 MHz have been reported. From a cw-pumped Nd:YAG laser capable of 10 W of cw power, peak powers of 570 W with a pulse duration of 25 ns have been obtained at a 2 MHz repetition rate [8.63].

The technique of cavity dumping is also employed in regenerative systems. In a regenerative laser a pulse is injected into a laser resonator containing an amplifier. The pulse passes several times through the same amplifier medium and is then switched out. Figure 8.32a shows an optical schematic of a laser which employs this technique [8.64]. The figure illustrates a diode-pumped Nd:YAG crystal located between two highly reflective mirrors, a Pockels cell Q-switch, and a polarizer. The Nd:YAG crystal is cw-pumped and repetitively cavity dumped at a 10 kHz repetition rate. During the 100 μs pump time, the Pockels cell is operated at zero wave retardation. This is the low Q-condition because radiation is transmitted out of the resonator through the polarizer. At the end of the pump pulse, the injection laser seeds a 8-ns pulse into the resonator through the rear reflector. At the same time, the Pockels cell is switched to 1/4 wave retardation which establishes the high Q-condition. Radiation is building up between the two highly reflective mirrors. The injected pulse is regeneratively amplified in the cavity for about 360 ns or 120 passes. The Q-switch is then returned

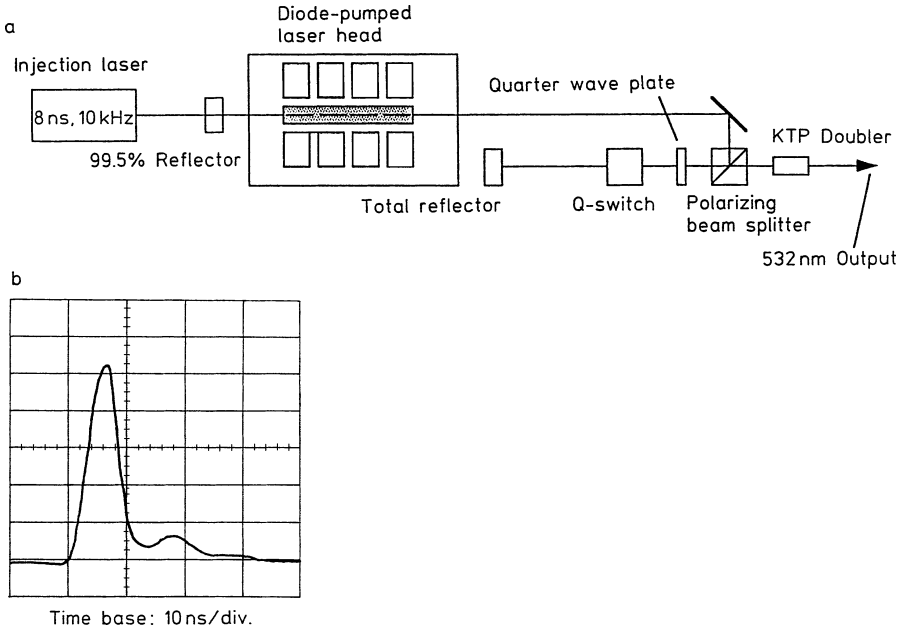

Fig. 8.32. Cavity dumping of an injection seeded laser. (a) Optical schematic of laser system and (b) output pulse shape

to zero wave retardation which dumps the amplified pulse through the polarizer. The KTP crystal converts the wavelength to 532 nm and shortens the pulse to about 5 ns. The sequence is repeated at a 10 kHz pulse repetition frequency. Figure 8.32b displays the output pulse at 532 nm.

An analysis of the extraction efficiency of cavity-dumped regenerative lasers can be found in [8.65]. The results are quite similar to the Q-switched case, and the extraction efficiency depends only on the amplifier gain and resonator losses.